

International Materials Reviews



ISSN: (Print) (Online) Journal homepage: https://www.tandfonline.com/loi/yimr20

Metal hybrids processed by high-pressure torsion: synthesis, microstructure, mechanical properties and developing trends

David Hernández-Escobar, Megumi Kawasaki & Carl J. Boehlert

To cite this article: David Hernández-Escobar, Megumi Kawasaki & Carl J. Boehlert (2021): Metal hybrids processed by high-pressure torsion: synthesis, microstructure, mechanical properties and developing trends, International Materials Reviews, DOI: <u>10.1080/09506608.2021.1922807</u>

To link to this article: https://doi.org/10.1080/09506608.2021.1922807

	Published online: 01 Jun 2021.
	Submit your article to this journal 🗷
ılıl	Article views: 22
Q	View related articles 🗹
CrossMark	View Crossmark data 🗹









Metal hybrids processed by high-pressure torsion: synthesis, microstructure, mechanical properties and developing trends

David Hernández-Escobar [©] a, Megumi Kawasaki [©] and Carl J. Boehlert [©] a

^aDepartment of Chemical Engineering and Materials Science, Michigan State University, East Lansing, MI, USA; ^bSchool of Mechanical, Industrial and Manufacturing Engineering, Oregon State University, Corvallis, OR, USA

ABSTRACT

The tradeoff between strength and ductility has long been identified as the 'Achilles' heel' of the mechanical properties in engineering applications. Metal hybrids processed by severe plastic deformation (SPD) have gained significant attention in recent years, as they have shown potential for enhancing strength and ductility simultaneously through different heterostructured designs. Among SPD processes, high-pressure torsion (HPT) is considered the most effective in grain refinement and offers excellent versatility for synthesising new materials with a wide variety of experimental setups and processing parameters. This review article describes the current state-of-the-art of metal hybrids processed by HPT, characterised by heterogeneous microstructures (i.e. nanoscale and/or microscale), through a comprehensive study of their synthesis-microstructure-property relationships. The potential of HPT-processed hybrids is highlighted and discussed along with their limitations. Suggestions are provided with the aim to advance current research trends towards future application in high-impact technologies, including the biomedical and microelectronic industries.

ARTICLE HISTORY

Received 2 August 2020 Accepted 22 April 2021

KEYWORDS

Heterogeneous microstructure; heterostructured material; high-pressure torsion; hardness; intermetallic compound; metal hybrid; nanocomposites; nanoindentation; post-deformation annealing; review; severe plastic deformation; strain rate sensitivity; ultrafine-grained

Introduction

Processing through the application of severe plastic deformation (SPD) methods is today a well-established tool for the fabrication of bulk ultrafine-grained (UFG) materials having grain sizes within the nanometre (10-100 nm) and sub-micrometer (100-1000 nm) ranges [1]. SPD processes encompass a series of metal forming techniques in which heavy straining is applied under high hydrostatic pressure, usually at room temperature (RT), leading to accumulated strains over $\sim 4-6$ [2]. Some of the major advantages of SPD methods are their capability to generate significant grain refinement without changing the overall dimensions of the sample. The resulting UFG microstructures, characterised by large volume fractions of high-angle grain boundaries, are ultimately responsible for the unique physical, mechanical and functional properties of SPD-processed materials, which cannot be attained by traditional deformation methods [3].

Though the roots of SPD metal processing can be traced back to the Han dynasty of ancient China in 200 B.C. [4], it was not until over 2000 years later that materials scientists invested significant research efforts to systematically develop the SPD techniques which current generations benefit from. In their analysis covering the period from 1980 to 1999, Lowe and

Zhu [5] discovered that very little research was published in the archival literature on the topic of SPD during the 1980s. However, they found 828 distinct publications on SPD between 1990 and 2002 (805 appearing in archival journals and 23 appearing in conference proceedings). There was a steady increase in the number of publications from 1990 through 2000, with the rate of publication nearly doubling between 2000 and 2001 [5]. Thus, one can estimate that the conception of modern-day SPD processing was around 1990, and there has been an explosion of research and development in this area ever since. In the 1990s and early 2000s, the SPD research evolved from investigating pure metals, to traditional metallic alloy systems, to more complex alloy systems [6,7]. More recently, SPD involving the joining of pure metals to produce metallic nanocomposite structures, referred to as 'hybrids', has emerged and is rapidly gaining significant momentum.

The scope of traditional thermomechanical processes, such as rolling, extrusion, forging, swaging, and drawing, is often limited by the strength-ductility tradeoff typically observed in engineering materials, which may be strong or ductile, but rarely both at once [7]. Unlike these deformation processes, SPD-processed materials are characterised by UFG microstructures containing large volume fractions of grain

boundaries (i.e. low- and high-angle boundaries), leading to the formation of interface-controlled materials [2]. As a result, a wide range of UFG metals and alloys have exhibited superior mechanical properties [8–16] (i.e. tensile strength, elongation-to-failure, fatigue, hardness, superplasticity) and functional properties [17-25] (i.e. electrical conductivity, magnetic resistance, hydrogen storage, photoluminescence, superconductivity).

The synthesis of metal hybrids using SPD techniques has gained notable interest over the last decade due to the resulting UFG microstructures, which exhibit a unique set of mechanical properties. Today, highpressure torsion (HPT) [26-28], equal channel angular pressing (ECAP) [29,30], and accumulative roll bonding (ARB) [31,32] are the most established SPD techniques. The foundations of HPT granted Bridgman the Nobel prize in 1946 [26], and it is considered the most efficient technique in terms of grain refinement. In addition, HPT offers versatility to explore the joining of different materials, alternative experimental designs, and processing parameters. The focus of this review article is set on HPT-processed metal hybrids, with emphasis placed on their synthesis routes, microstructural characteristics, as well as their resulting mechanical properties and future perspectives.

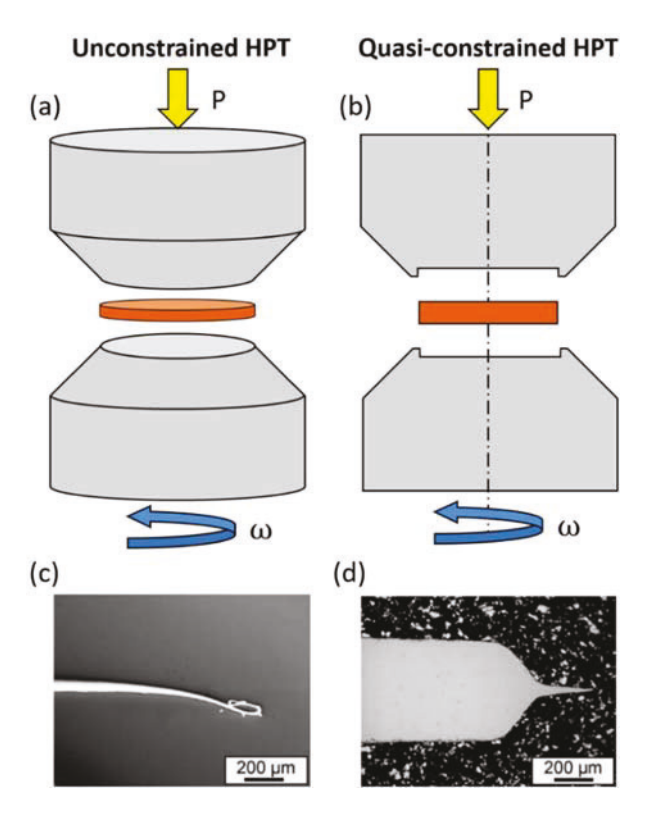


Figure 1. Schematic setup of (a) unconstrained HPT and (b) quasi-constrained HPT, where P indicates the applied pressure and ω indicates the rotational speed. The appearance of the peripheral cross-section of samples produced by (c) unconstrained HPT applied to pure Cu for 5 turns and (d) quasi-constrained HPT applied to pure Fe for 5 turns. Adapted from [33].

During HPT, a disk shaped specimen (typically 10-20 mm diameter and 1 mm thickness) is simultaneously subjected to a large hydrostatic pressure (usually 6 GPa) and severe torsional straining, as shown schematically in Figure 1(a). This shows an idealised version of HPT, where the lack of lateral constraints prevents a uniform applied pressure, thereby leading to a continuous decrease in sample thickness, as observed in Figure 1(c). In contrast, a constrained version of HPT would theoretically lead to pure torsion deformation under hydrostatic pressure without altering the sample geometry; however, it is practically impossible as it assumes a frictionless condition. A trade-off between these two versions, quasi-constrained HPT, which includes a cylindrical cavity in each anvil that is slightly shallower than the HPT sample, is the most frequently used HPT setup, see Figure 1(b). In this manner, a small amount of material flows out of this cavity, as shown in Figure 1(d), ensuring a uniform sample thickness over the majority of the sample diameter under a nearly ideal hydrostatic pressure during torsion [33].

The action of concurrent compressive and shear stresses introduces a significant amount of point and line defects within the specimen, which enhances atomic diffusion even at RT [34]. As shown in Equation (1), the shear strain (γ) in the disk specimen during HPT can be expressed in terms of the number of rotations (N), the distance from the centre of the disk (r), and the disk thickness (h) [35]. The equivalent Von Mises strain (ε_{eq}) can be then calculated using Equation (2) for $\gamma < 0.8$, and Equation (3) for $\gamma \ge$ 0.8 [6,36]:

$$\gamma = \frac{2\pi Nr}{h} \tag{1}$$

$$\varepsilon_{eq} = \frac{\gamma}{\sqrt{3}} = \frac{2\pi Nr}{h\sqrt{3}}$$
 (for $\gamma < 0.8$) (2)

$$\varepsilon_{eq} = \left(\frac{2}{\sqrt{3}}\right) \ln \left[\sqrt{\left(1 + \frac{\gamma^2}{4}\right)} + \frac{\gamma}{2}\right] \quad \text{(for } \gamma > 0.8)$$
(3)

Despite the significant grain size refinement achieved by HPT, often to the nanoscale range (1–100 nm), the resulting strengthening increase is limited by a steady-state regime reached at high strain values (i.e. 8-10 effective strain) [37]. Thereby, grain size saturation limits the strength increase in HPTprocessed metals and alloys having uniform microstructures. Consequently, a modification of the conventional HPT process, able to promote solid-state reactions through direct diffusion bonding at RT, has been investigated for synthesising multiple metal hybrid systems, including Al-Cu [38-40], Al-Mg [41-47], Al-Fe [46], Al-Ti [46], Cu-Ta [48], Cu-ZnO [49], Fe-V [50,51], Zn-Mg [52-54] and V-Zr [55].

These hybrids can be defined as metal-based composites, comprised of at least two elements, whose final properties are determined by their unique nanoscale architecturing, which in turn is achieved through mechanical bonding of dissimilar bulk metals by HPT processing.

This article offers a comprehensive review of the experimental procedures used to synthesise HPT hybrid systems, as well as their resulting ultrafinegrained (UFG) microstructures and mechanical behaviour. The flowchart presented in Figure 2 aims to guide the reader through the organisation of the paper and how each of the major sections is in turn subdivided into separate topics, as summarised below.

The different approaches used to produce HPTprocessed hybrids are covered in "Synthesis of hybrid metal systems by HPT". Particular attention is given to the mechanical bonding of dissimilar bulk metals (i.e. Al-Cu, Al-Mg, Zn-Mg systems) in "Origin of the mechanical bonding of dissimilar metals" and the variety of sample configurations investigated to date in "Sample formats of HPT-processed hybrids". One of the limitations of conventional HPT, its small sample size, together with recent promising attempts to upscale the HPT procedure, are discussed in "Upscaling HPT and size limits of hybrid samples". Additional synthesis approaches based on HPT principles, including the consolidation of powders and machining chips, are presented in "Other strategies for synthesising metal hybrids using HPT".

The mechanisms governing the microstructural evolutions of metal hybrids obtained by HPT are presented in "Microstructural evolution of HPT-processed metal hybrids", which is organised as follows. The microstructural features common to most hybrid systems synthesised by HPT, are discussed in "General microstructural evolution in HPT hybrid systems". The formation of additional microstructural features of interest, only observed in particular hybrid systems, is reported in following subsections. The nucleation of intermetallic compounds, and the critical contributing factors for their formation during HPT, are presented in "Insitu nucleation of intermetallic compounds". The microstructural effects of post-deformation annealing (PDA) treatments in the different hybrid systems are discussed in "Effect of post-deformation annealing". The major contributing factors leading to HPTinduced supersaturated solid solutions (SSSS) are summarised in "Formation of supersaturated solid solutions". Additional microstructural-related topics of interest, such as amorphisation and thermal stability, are reported in "Other microstructural transformations in HPT-processed hybrids".

The effect of the microstructural evolutions on the mechanical performance of HPT-processed hybrids is presented in "Micro-mechanical properties of HPTprocessed metal hybrids", which is subdivided as follows. "Hardening mechanisms of HPT hybrids obtained from mechanical bonding" presents the hardness evolution during HPT and PDA in different hybrid systems, as well as the major strengthening mechanisms involved in such evolutions. A discussion on the "Evaluation of global mechanical properties from HPT hybrids" is introduced, together with a general recommendation for current researchers to enable a more comprehensive analysis of the processingmicrostructure-property relationships. An evaluation of the plastic deformation behaviour of HPT hybrids from nanoindentation studies is presented in "Nanoscale plastic deformation and strain-rate sensitivity of HPT hybrids", highlighting the effect of PDA, which enhances both hardness and strain-rate sensitivity in the Zn-Mg hybrid system. The general requirements "Towards strength-ductility synergy through heterogeneous microstructures" in HPT-processed hybrids are also presented. Lastly, the potential and feasibility of HPT to produce metal hybrids for tailored engineering applications is discussed in "Future potential applications of HPT-processed components", with emphasis placed on biomedical implants, microelectronics, magnetic materials, and hydrogen storage.

Synthesis of hybrid metal systems by HPT Origin of the mechanical bonding of dissimilar metals

A wide variety of synthesis approaches has used severe plastic deformation (SPD) principles to obtain hybrid materials through the mechanical bonding of dissimilar metals. Before focusing on these approaches involving HPT, it is worthwhile to describe how mechanical achieve bonding has been used to microstructures.

Clad rolling produces a single multilayered sheet via elevated temperature rolling of individual metal sheets stacked on top of each other. This process reduces the grain size to the microscale range (i.e. 0.1-1 µm), thereby increasing the strength, but only to a limited extent. To further refine the microstructure, this process can be repeated multiple times by cutting the rolled material in half at the end of each rolling pass and subsequently restacking, followed by further rolling. This sequential process defines the so-called ARB, a popular SPD technique used to produce UFG metal sheets. ARB, which is commonly performed on FCC metals due to their relatively slow work hardening [56], has also been used to fabricate metal hybrid sheets. For instance, multilayered hybrids with compositions of Al/Ni [57], Al/Mg [58], Al/Ti [59], Al/Al-Zn-Mg-Cu [60], and Cu/Ta [61], have been successfully ARB-processed. However,



Figure 2. Flowchart showing the organisation of this review paper in different sections, and the contents covered in each of them.

the inherent microstructural and mechanical anisotropy between the rolling and transverse planes of ARB sheets [62], along with the fact that it requires continuous supervision during processing to ensure good material bonding (i.e. surface brushing and decontamination between rolling steps), motivated research and development of alternative SPD processes, like HPT, for producing metallic hybrids. The accumulated plastic strain during HPT is generally higher than that for ARB [63], thereby resulting in a more efficient production of metallic hybrids at RT.

Sample formats of HPT-processed hybrids

Metal hybrids have been synthesised by HPT using a variety of sample formats and experimental parameters. The final dimensions of the HPT-processed metallic hybrids can be identical to those fabricated

from conventional HPT processing of pure metals or alloys (common dimensions being 10 mm diameter and 1 mm thickness). However, unlike that for conventional HPT processing of pure metals and alloys, where a single disk is used (Figure 3(a)), the synthesis of HPT hybrids offers a variety of possible layered formats that can be customised for obtaining tailored microstructures and mechanical properties. Some of these formats are illustrated in Figure 3(b–d), and the experimental parameters used to produce specific metallic hybrid systems are described below.

Sun et al. [64] showed that HPT was a feasible technique to mechanically bond half disks to produce bulk metallic glass matrix composites. A year later, the feasibility to produce mechanical bonding between dissimilar bulk metals through HPT at RT was demonstrated by two independent research groups: Sun et al. [65] (through the combination of Cu/Zr, Cu/Ni, and Cu/

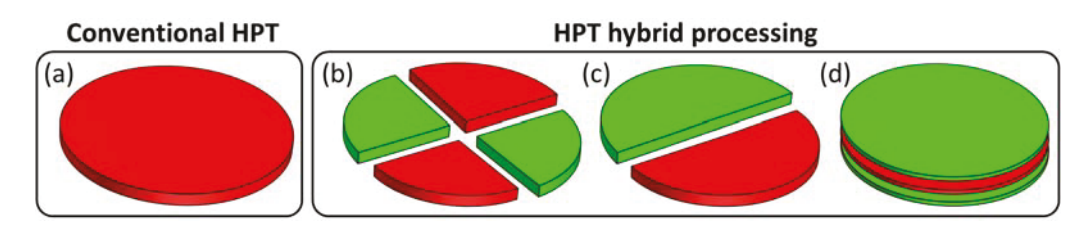


Figure 3. Sample formats used in (a) conventional HPT and (b–d) HPT hybrid processing: (b) quarter-disk, (c) half-disk and (d) stack-disk.

Ag half disks) and Miyazaki et al. [66] (through the combination of Ag/Ni and Nb/Zr half disks). Both groups used the experimental setup illustrated in Figure 3(c). The following year, the combination of four alternate quarter disks of Al-6061 alloy and pure Cu, as seen in Figure 3(b), was demonstrated by Bouaziz et al. [67], where 1 turn under 2.5 GPa resulted in the joining of the two materials into a single bulk disk with an average grain size (GS_{ave}) of 100-200 nm. Later, solid-state reactions between two alternate Al and Cu half disks were confirmed by Oh-ishi et al. [38] after HPT processing for 1, 10, and 100 turns with 6 GPa, see Figure 3(c). The increased number of rotations with respect to the previous study led to the formation of nanoscale Al-Cu intermetallic phases, namely Al₂Cu, AlCu, and Al₄Cu₉, as well as the dissolution of Al and Cu in the matrix due to the enhanced atomic diffusion. These two studies demonstrated that HPT was not only capable of achieving mechanical bonding between different metals and metallic alloys, but also imposing significant microstructural changes. However, given the complexity associated with the arrangement and alignment of the quarter-disks and half-disks in the HPT anvils before processing, alternative less-complex sample formats were investigated thereafter.

A more straightforward approach to produce mechanical bonding was then introduced, which consisted of stacking different metal disks without any surface adhesion or brushing treatment prior to HPT processing. This sample format was originally developed by Ahn et al. [68] in 2015 for three metallic disks stacked alternatively in an A/B/A sequence, where the top and bottom material (A) was different from that in the centre (B), as sketched in Figure 3 (d). The first hybrid system to be synthesised by HPT using this approach was Al/Mg/Al, which was subjected to 6 GPa for 5, 10, and 20 turns [42,45,68,69]. Similar to the Al-Cu HPT-processed hybrids mentioned earlier, the resulting Al-Mg hybrids exhibited a nanoscale matrix grain structure as well as nanoscale intermetallic compounds, namely Al₃Mg₂ and Al₁₂Mg₇. Since then, several other HPTprocessed hybrid systems have been investigated, such as Al-Cu [38-40], Al-Mg [42,44,45,69,70], Al-Fe [46], Al-Ti [46], Cu-Ta [48], Cu-ZnO [49], Fe-V [50,51], Zn-Mg [52-54] and V-Zr [55]. This stacking approach is now routinely used to produce metallic hybrids due to their versatility and adaptability for use by almost all metal systems without the need for a binder (which is sometimes required for other joining techniques, including those based on additive manufacturing). The resulting microstructural evolution and mechanical properties, as well as the ease for controlling the final composition by simply adjusting the thickness and/or the number of the disks in the stacking sequence, are the primary reasons that make HPT a unique approach for synthesising metal hybrids.

Upscaling HPT and size limits of hybrid samples

One of the disadvantages of HPT to process metal hybrids is the large applied pressures (i.e. generally, 6 GPa) required to mechanically bond the different metallic disks. The means and expenses required to generate such large pressures limit the size of the HPT-processed samples, which are typically 10 mm diameter and 1 mm thickness, though diameters as large as 20 mm have also been fabricated [71,72]. One of the reasons why such large forces or pressures are needed is to avoid slip of the materials in the HPT equipment during deformation. For example, 8 GPa pressure (equivalent to 40 tons pressure) was required to successfully process an 8 mm diameter and 0.8 mm thickness W-25Cu (wt. %) nanocomposite by HPT [73]. Another reason why larger forces or pressures are needed is to obtain both uniform grain sizes and mechanical properties (i.e. hardness) between the centre and periphery of the HPT-processed disk. Work by Zhilyaev et al. [6,74] portrayed results from Ni disks after HPT for 5 turns at applied pressures of 1, 3, 6, and 9 GPa. The results showed that an increase in the applied pressure from 1 to 9 GPa gives an overall increase in the Vickers microhardness (HV), especially at the centres of the disks, where the strain is lower than at the periphery. At 9 GPa, uniform hardness values were exhibited from the centre to the periphery of the disk. These measurements supplemented by transmission electron microscopy (TEM) examination of the microstructures. After 1 GPa pressure, there was a significant discrepancy between the finer grain sizes at the periphery of the disk and the larger grain sizes in the centre of the disk. After 3 GPa pressure, although there was less inconsistency in grain size, there was a morphological difference where the periphery grains were equiaxed while the centre grains were elongated. Only after 9 GPa pressure, the microstructure was consistent with respect to both grain size and morphology. Thus, 6 GPa was considered to be a reasonable pressure to obtain both uniform grain sizes and hardness values across the HPT-processed materials, and this has been adopted as the accepted pressure used in most studies.

There are significant implications associated with the scalability of HPT manufactured components. Although it is possible to produce HPT disks larger than 10 mm diameter and 1 mm thickness, the investment in research and industrial infrastructure required is considerable, and therefore the benefits of implementing this upscaled machinery need to scale accordingly. One means to reduce the forces necessary for successful HPT bonding is by increasing the temperature. However, this results in additional costs for heating and can result in the ingress of undesirable diffusion products, such as O, N, C, and H, as well as the possibility of imposing undesirable phase transformations, recrystallisation, and grain growth, which can lead to reduced strengths, thereby defeating one of the main benefits of HPT processing. For example, HPT-processed W-25Cu (wt. %) at 400°C resulted in significantly larger W particles than those observed after HPT processing at RT [73]. In order to overcome the reputation of HPT as a merely academic curiosity, much effort over the last few years has focused on upgrading HPT machinery for producing larger samples. The feasibility of RT HPT to obtain cylindrical samples, having 10 mm diameter and 8 mm thickness, was confirmed in an Al-Mg-Sc alloy processed under 1 GPa applied pressure for ¼ and 1 turn [75]. However, it was found that the deformed microstructure after 1 turn was inhomogeneous across the thickness and exhibited notable variations in the HV values throughout different samples. Thus, a greater number of turns and a higher applied pressure (consistent with the previous discussion) is needed to increase the strains imposed and obtain a more homogeneous fine-grained microstructure.

There are two conditions that must be simultaneously met in order to obtain an HPT sample with a homogenous ultrafine-grained (UFG) microstructure. First, the saturation strain (i.e. strain value above which the grain size remains constant) must be achieved. Second, a certain thickness (t) to diameter (d) ratio, t/d, must be obtained. For example, t/d $d \le 1/13$ for HPT-processed American Rolling Mill Company pure iron (Armco-Fe) was required to achieve both axial and radial microstructural homogeneity [33]. However, this t/d value may not be universally applied to all materials and may vary for different compositions.

The size and shape of the initial disk material (prior to HPT processing) can be adjusted, provided the following technical aspects are met. First, the applied pressure must be sufficient to prevent sliding between the sample and the anvils during torsional straining. Generally, this pressure should be at least three times greater than the material's yield stress, and the maximum pressure is determined by the hardness of the HPT anvils. Second, the torque required to enable torsional straining of the sample under fully-plastic flow is proportional to d³; hence, more powerful motors are required for samples with larger diameters. The anvil diameter must be increased accordingly to withstand higher torques [76]. Taking into account these concepts, conventional HPT machines can be adapted to produce larger samples. To date, the largest samples to be HPT processed, 60 mm in diameter and 12 mm thick, were synthesised using a machine with

10,000 kN maximum loading capacity and 130 kN·m maximum torque [77].

The feasibility of scaling-up the dimensions of an Al/ Mg/Al multilayered HPT hybrid was recently investigated, and the associated effects on the microstructure and mechanical properties were reported [47]. The study concluded that the microstructures of Al-Mg hybrid samples, having 25 mm diameter and 2 mm thickness, were comparatively similar to those of conventional samples with 10 mm diameter and 1 mm thickness after 10 and 20 turns. Both sample dimensions exhibited a similar change in hardness values across their cross-section and thickness. In order to prevent the excessive temperature rise from plasticity-induced heating, the rotational speed was adjusted from 1 rev min⁻¹ in the conventional sample to 0.4 rev min⁻¹ in the upscaled one. Despite this decrease in rotational speed, indications of microstructural recovery were observed at the disk periphery of the larger sample. To date, this is the only study that has reported scale-up attempts for HPT hybrids.

Motivated by overcoming the scalability limit of the HPT process, several researchers have recently made substantial efforts for developing similar severe plastic deformation (SPD) methods that can maintain the extensive grain refinement of HPT in larger samples. Fujioka and Horita [78] introduced the high-pressure sliding (HPS) process in 2009, whose setup combines two anvils and one plunger in between, such that rectangular metallic sheets can be placed between the anvils and the plunger. Compressive forces are applied to the anvils during plunger displacement normal to the compression direction (i.e. parallel to the anvil surface), such that large shear strains are introduced in the sheet samples. HPS-processed sheets can reach dimensions of 10-30 mm width, 100 mm length, and 1 mm thickness, and exhibit grain sizes in the range of 200-300 nm [79]. In 2019, Toth et al. [80] developed high-pressure compressive shearing (HPCS), a modified version of HPS with the addition of a confining pressure and a higher compressive pressure for introducing higher shear strains. Similarly, Edalati and Horita [81] developed continuous high-pressure torsion (CHPT) in 2010 as an attempt to produce microstructural refinement in metal sheets continuously. Undoubtedly, there is a notable interest in adapting HPT principles for upscaling and continuous processing for industrial feasibility while maintaining its extraordinary grain refinement.

Other strategies for synthesising metal hybrids using HPT

In addition to the approaches covered in previous sections to process HPT hybrids from direct mechanical bonding of bulk materials, other alternative methods have explored the feasibility of HPT to consolidate materials in the form of powders or machining chips. In either case, the material can be filled into the cavity formed between the HPT anvils to produce a compact solid sample at room temperature (RT).

Consolidation of powders via HPT has been used to produce a variety of metal-matrix and ceramic-matrix composites. Different combinations of miscible alloy systems (i.e. binary Al-Mg [82] and Al-Fe [83]) and immiscible alloy systems (i.e. binary Cu-Fe [84] and Au-Fe [85], or ternary Cu-Fe-Ag [86] systems) have been consolidated via HPT from metallic powder mixtures, resulting in single-phase or dual-phase nanocrystalline microstructures. Ceramic-reinforced metal-matrix composites have been also successfully consolidated from powders at RT, including Cu-SiO₂ [87], Al-Al₂O₃ [87,88], Ti-TiO₂ [89], Co-NiO [90], Co-Al₂O₃ [91], Mg-MgO [92]. For instance, Ashida et al. [88] produced an Al-30Al₂O₃ (vol. %) nanocomposite, of 10 mm diameter, from pure Al powder (150 µm particle size) and Al₂O₃ powder (30 nm particle size) using HPT for 10, 20, and 50 turns, under 1 rev min⁻¹, 6 GPa, and RT. The resulting microstructure consisted of an Al matrix, with a GS_{ave} of ~ 550 nm after 50 turns, containing dispersed Al₂O₃ nanoparticles. Metal-based composites reinforced with carbon allotropes, such as graphene [93-96] and fullerenes [97–100] (i.e. carbon nanotubes (CNT)), have also been synthesised from powder consolidation using HPT. Lastly, some examples of ceramic-matrix composites that have been fabricated via HPT from powder mixtures are ZrO₂-Y₂O₃ [101], WC-Co [102], TiO₂-ZnO [103], and GaN-ZnO [104].

Machining chips have also been consolidated into compact samples using HPT at RT [105-108]. The use of metal chips offers an opportunity to recycle a material that already underwent plastic deformation, and as such, contains a higher dislocation density than its unmachined counterpart. For instance, a Mg-10Al₂O₃ (vol. %) composite was produced by the consolidation of pure Mg chips and Al₂O₃ microparticles [105]. The mixture was precompacted at 250 MPa into disks of 10 mm diameter and 1 mm thickness and then processed by HPT under 6 GPa at 1 rev min⁻¹ for 1/8, 1, and 5 turns. This study demonstrated an adequate bonding between chips and particles and a good mixing of the different phases after 5 turns, which resulted in a composite with a reasonably homogeneous microstructure. In another study, Al-8Si-3Cu (wt. %) chips were pre-compacted at 200 MPa and then consolidated into a composite, with 10 mm diameter and 1 mm thickness, via HPT under 8 GPa at 1 rev min⁻¹ for 10 turns [107]. The HPT process resulted in dense bulk composite samples (i.e. 99.6% relative density) with a higher and more homogeneous microhardness distribution than that of the HPT-

processed alloy counterpart due to the higher imposed plastic strain.

Microstructural evolution of HPT-processed metal hybrids

General microstructural evolution in HPT hybrid systems

Processing of HPT hybrids through the mechanical bonding of several stacked metal disks, as shown in Figure 3(d), leads to a general good bonding between the separate disks into a compact sample at relatively low strain (i.e. 1 turn), without noticeable cracks, voids, or segregations. As observed in the scanning electron microscope (SEM) images in Figure 4 for different HPT hybrid systems, increasing torsional straining results in a disruption of the multilayered structure after 1 turn, followed by a subsequent phase fragmentation with increasing number of turns. In some metal systems, HPT leads to compositional mixing in such a way that new phases and/ or intermetallic compounds nucleate in the microstructure, as is the case of the Al-Cu, Al-Mg and Zn-Mg systems shown in Figure 4(a-c), respectively. However, other metal systems, such as Al-Fe and Al-Ti, shown in Figure 4(d,e), respectively, do not exhibit any phase transformation despite the fragmentation of the multilayered structure after severe torsional straining.

Al-Cu HPT hybrids have been synthesised at RT under 6 GPa, at 1 rev min⁻¹, for 10, 20, 40, and 60 turns [39]. The microstructure analysis after HPT demonstrated an ultrafine-layered structure with a GS_{ave} ~ 80 nm after 20 turns and an equiaxed microstructure with a $GS_{ave} \sim 30 \text{ nm}$ in the peripheral regions of the disk after 60 turns. However, relatively large Al-rich and Cu-rich phases were still present within the central regions of the disk after 60 turns, as observed in Figure 4(a). It was apparent that after 60 turns, the Cu-rich phase was fully dissolved into the Al-rich matrix, and there was no evidence of phase segregation, as observed in Figure 5(a). Three different intermetallic compounds, namely Al₂Cu, AlCu, and Al₄Cu₉, were identified after 20 turns, as observed in Figure 5(b), which gradually increased in volume fraction after 40 and 60 turns.

Al-Mg HPT hybrids have been processed at RT under 6 GPa, at 1 rev min⁻¹, for 1, 5, 10, 20, 40, and 60 turns [43,68]. Microstructural analysis revealed a significant grain refinement after 5, 10, and 20 turns, with a $GS_{ave} \sim 190 \text{ nm}$, $\sim 90 \text{ nm}$, and $\sim 60 \text{ nm}$, respectively. The disk after 10 turns revealed the presence of two intermetallic compounds in the regions of higher plastic deformation; Al₃Mg₂ in the form of ~ 30 nm nanolayers, and $Al_{12}Mg_{17}$ in the Al-rich matrix, which was in a SSSS state, as shown in Figure 5(c).

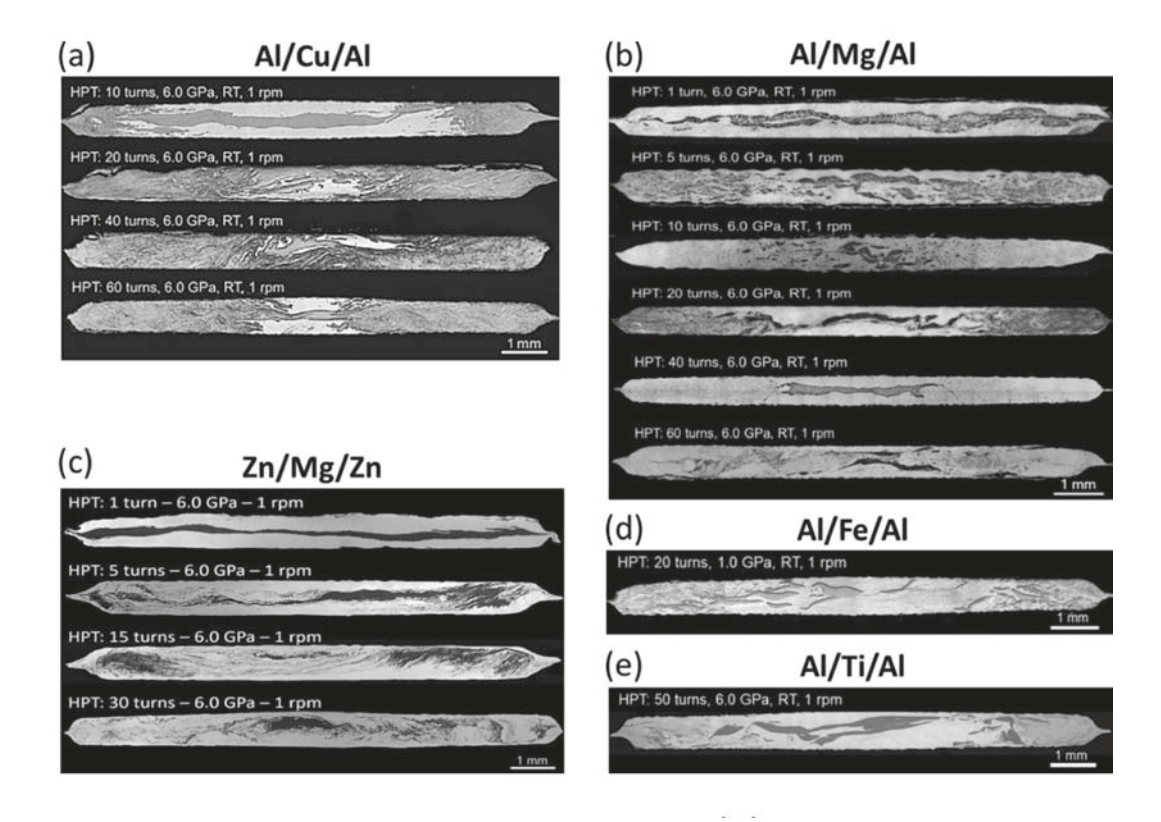


Figure 4. SEM images of the cross-sections of different A/B/A-type hybrids processed by HPT at RT under an applied pressure between 1 and 6 GPa, a rotational speed of 1 rev min⁻¹ for increasing number of turns. (a) Al/Cu/Al, (b) Al/Mg/Al, (c) Zn/Mg/ Zn, (d) Al/Fe/Al and (e) Al/Ti/Al. Reproduced with permission from [39,42,44,46,52].

Further HPT processing for 40 and 60 turns resulted in a slight decrease of the GS_{ave} to \sim 40 nm and \sim 30 nm, respectively, and the dissolution of both Al₃Mg₂ and Al₁₂Mg₁₇ in the Al-rich matrix, as observed in Figure 5(d). This was associated with an increased Mg concentration in the Al-rich matrix after 40 and 60 turns, which occurred due to enhanced diffusion of Mg in the intermetallic compounds.

Zn-Mg HPT hybrids were obtained at RT under 6 GPa, at 1 rev min⁻¹, for 1, 5, 15, and 30 turns [52]. The microstructural characterisation of the HPT-processed disks showed the formation of a sub-micron multilayered structure embedded in a Zn-rich matrix with a GS_{ave} of ~ 600 nm at the disk periphery after 30 turns. The grain refinement from 1 to 15 turns was accompanied by a significant increase in the volume fraction of high-angle grain boundaries. The slight increase in GS_{ave} after 30 turns, together with a significant decrease of the basal texture intensity, suggested the occurrence of dynamic recrystallisation (DRX) during HPT. Nanosized intermetallic compounds Mg₂Zn₁₁ and MgZn₂ were identified near to the disk edges after 15 and 30 turns, and their volume fractions increased consistently with the number of turns, as observed in Figure 5(e,f). Similar to the Al-Cu and Al-Mg systems, the central region of the Zn-Mg hybrid disk after the highest number of rotations (i.e. 30 turns) exhibited larger phases than the peripheral regions, as observed in Figure 4(c).

The extreme grain refinement achieved in the Al-Cu, Al-Mg, and Zn-Mg HPT hybrid systems, along with the nucleation of different intermetallic compounds, had a strong effect on their mechanical perdetailed "Micro-mechanical formance, in HPT-processed properties of hybrids". However, Al-Fe and Al-Ti HPT hybrids did not exhibit any compositional mixing despite the phase fragmentation at increasing number of turns, and thus, no additional intermetallic compounds were formed in these cases. This can be observed in the X-ray diffraction (XRD) patterns of the Al-Fe hybrid after HPT for 20 turns and the Al-Ti hybrid after HPT for 50 turns, which are depicted in Figure 6(a,b), respectively. As a consequence, hardness measurements in the Al-Fe and Al-Ti hybrid systems reached maximum values of 330 and 350 HV, respectively, which are consistent with the saturated hardness exhibited by pure Fe and Ti when processed separately by HPT without any phase transformation [46,109].

Mechanical bonding of dissimilar metals by severe shearing can introduce metastable phases, including intermetallic compounds and supersaturation phases nucleated at the vicinity of the interfaces of dissimilar metals. The mechanisms of such phase transformations, which are covered in following sections, can be understood through the formation of tribomaterials [110], which involve the formation of unique flow patterns, similar to the flow of liquids. These

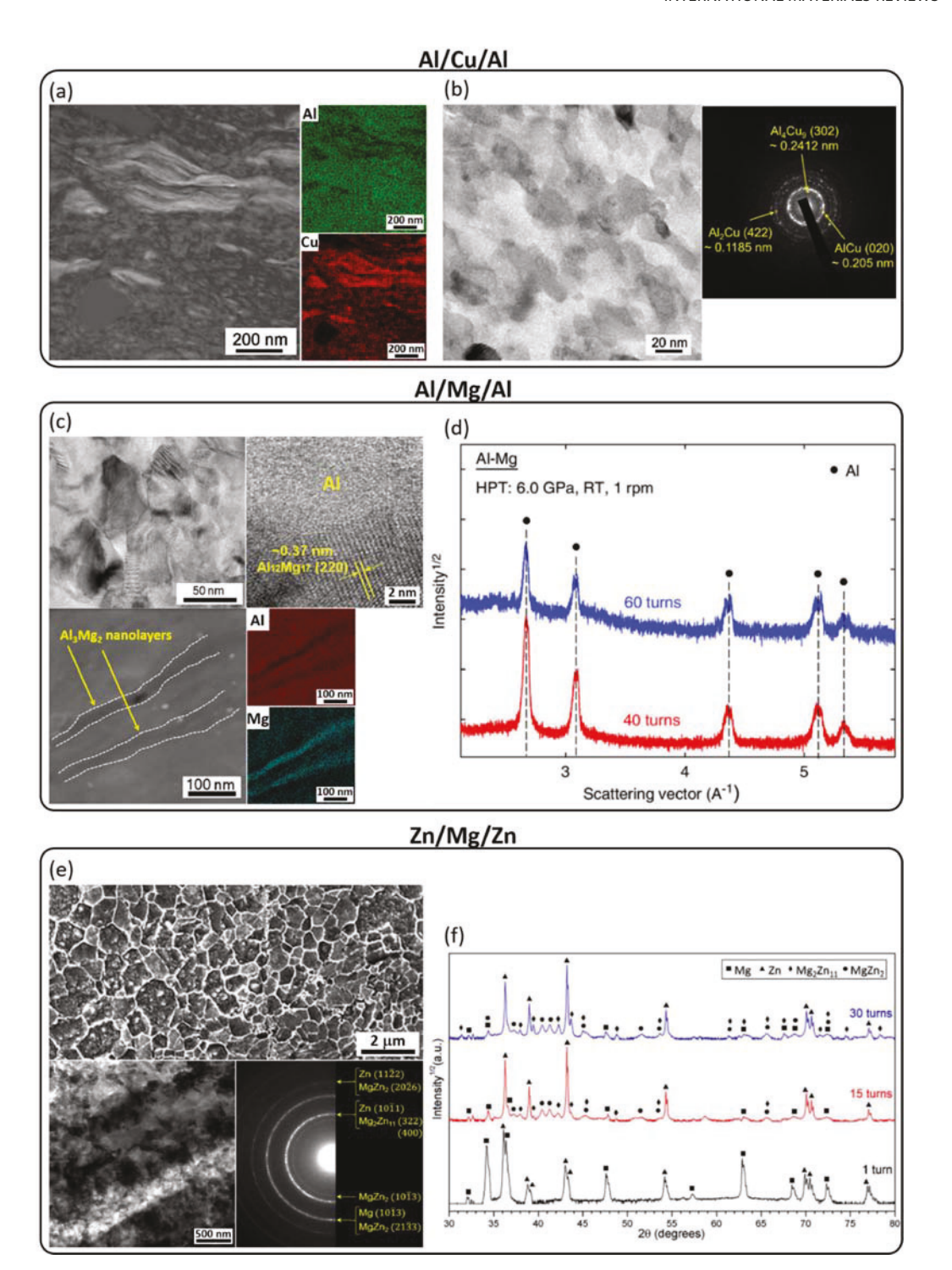


Figure 5. Representative microstructures of Al-Cu, Al-Mg, and Zn-Mg HPT hybrids. Al-Cu system after HPT for 60 turns: (a) SEM image with EDS elemental maps of Al and Cu, (b) TEM micrograph and corresponding SAED pattern. Al-Mg system after HPT for 10 turns: (c) TEM micrographs and corresponding EDS elemental maps of Al and Mg, (d) XRD patterns after 40 and 60 turns. Zn-Mg system after HPT for 30 turns: (e) SEM and TEM with corresponding SAED pattern, (f) XRD patterns after 1, 15, and 30 turns. Reproduced with permission from [39,43,52,68].

patterns appear as vortices adjacent to the interfaces when a Kelvin–Helmholtz (K–H) shear instability [111,112] occurs under shear or sliding deformation and can be further accelerated under high-pressure processing. Thus, the interfaces in the mechanically bonded metals experience severe shear, and this introduces, through the K–H instability, large volumes of tribomaterials with nano-scale grains during the phase mixture and grain refinement by HPT.

In-situ nucleation of intermetallic compounds

As anticipated from the discussion in the previous section, several HPT hybrid systems (i.e. Al-Cu, Al-Mg, and Zn-Mg) were found to promote the nucleation of intermetallic compounds. However, other HPT hybrid systems (i.e. Al-Ti and Al-Fe) did not exhibit any evidence of intermetallic formation. This section presents the critical conditions for the formation of

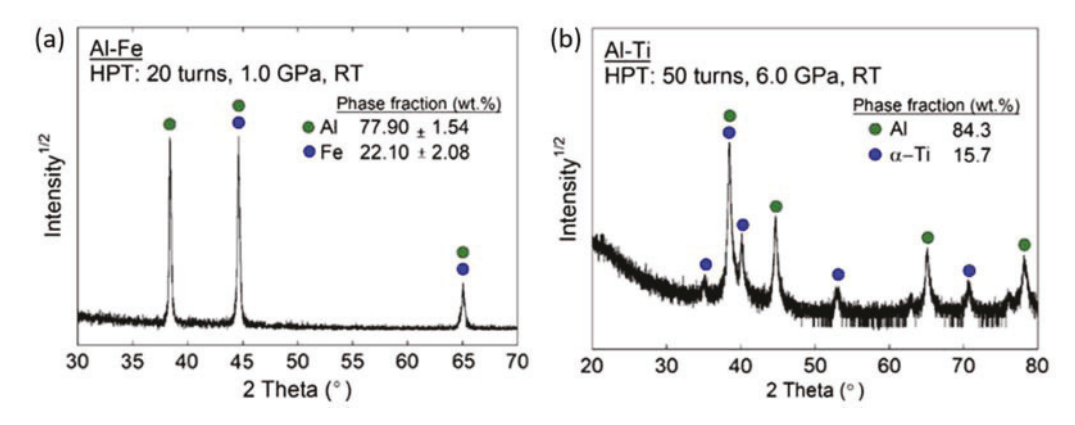


Figure 6. XRD profiles of the (a) Al-Fe HPT hybrid after 20 turns at 1 GPa and (b) Al-Ti HPT hybrid after 50 turns at 6 GPa. Reproduced with permission from [46].

intermetallics under plasticity-driven mechanisms, and rationalises why different hybrid systems are (or are not) able to nucleate intermetallic compounds during HPT processing.

The major contributing factor to the formation of intermetallic compounds during mechanical bonding of dissimilar metals is an enhanced atomic diffusion at the large plastic strains achieved in HPT processing, which is due to a significant increase in the concentration of point defects. Different mechanisms involving enhanced atomic mobility have been proposed to explain the shear-induced chemical mixing in heterogeneous microstructures [113–116], like those obtained after processing the HPT hybrids. Dissolution becomes energetically favourable, from a thermodynamic viewpoint, when the phase size decreases to the nanometre level. Thereby, the formation of a solid solution can be achieved through mechanical mixing by dispersing the dissolved atoms in the matrix. Another

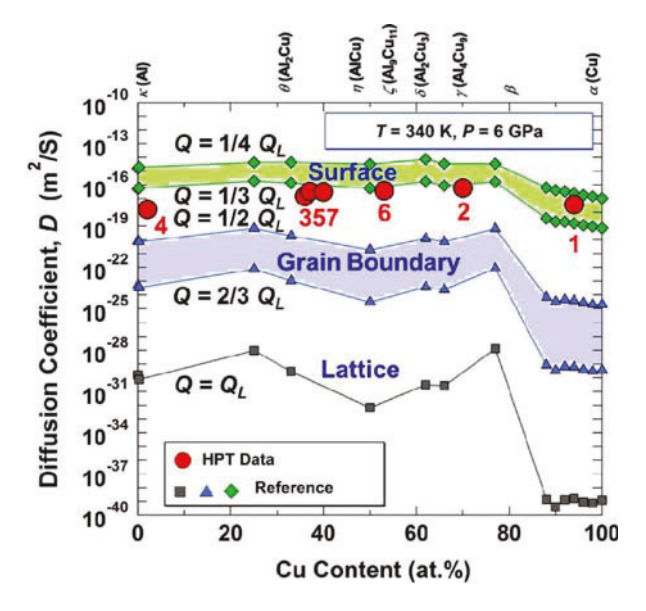


Figure 7. Comparison of the diffusion coefficients estimated for the Al-Cu HPT hybrids as a function of the Cu concentration (red points 1-7) against those corresponding to the Al-Cu alloy system (reference values). Reproduced with permission from [38].

mechanism suggested by Veltl et al. [117] claimed that the energy stored in the grain boundaries of ultrafine-grained (UFG) microstructures serves as the driving force for solid solution formation. In contrast, Bellon and Averback [118] proposed a plasticity-driven mechanism, known as the kinetic roughening model, which suggested that atoms are shifted across the interphases of the phase boundaries by the shear of atomic glide planes. That is, during shearing of the glide planes, the phase boundaries become increasingly rough, leading to microstructural refinement and eventually to complete chemical mixing of the multiphase system. The synthesis of metastable phases during severe plastic deformation (SPD) was explained by Straumal et al. [119] using the effective temperature model, originally developed for materials under irradiation. This model assumes that the SPD material's microstructure is converted into a separate microstructural state that could be described by a specific increased temperature, and this allows for a prediction of the structure and composition of phases formed during SPD.

Several studies have shown experimental evidence for the accelerated atomic diffusion during SPD, which seems to be the key factor to enable the mechanisms and models summarised above. For instance, a Cu-Pb alloy processed by ECAP demonstrated increased atomic mobility, which was attributed to the introduction of additional free volume (i.e. the volume that is not occupied by atoms) during severe straining, in the form of non-equilibrium interfaces, vacancy clusters, nanovoids, and micropores [120]. An estimation of the diffusion coefficients of the Al-Cu HPT hybrids revealed that they were about 10¹²-10²² times larger than those of lattice diffusion, and comparable to those of surface diffusion in the Al-Cu alloy system [38], as shown in Figure 7. This was suggested to be the reason for the formation of Al₂Cu, AlCu, and Al₄Cu₉ intermetallic phases in the Al-Cu HPT hybrid system. The nucleation and increased volume fractions of Mg₂Zn₁₁ and MgZn₂ intermetallics in the Zn-Mg HPT hybrids were consistent with a decrease of the matrix Mg-phase volume

fraction from 15 to 30 turns [52,53]. These intermetallics were consistently identified by XRD, as shown in Figure 5(f), and by Fast Fourier Transform (FFT) analysis of HRTEM images, as shown in Figure 8. Moreover, it was observed that the fraction of MgZn₂ was greater than that of Mg₂Zn₁₁ after 15 turns, contrary to what was expected from their formation enthalpies. Given that MgZn₂ requires about twice the amount of Mg atoms than Mg₂Zn₁₁, and that intermetallics were predominantly found in Mgrich areas, the atomic availability for the intermetallic formation plays a particularly important role when complete chemical mixing has not been obtained. However, the fraction of Mg₂Zn₁₁ increased at the expense of MgZn₂ after post deformation annealing, in agreement with their formation enthalpies, thereby providing a more thermodynamically favourable energy state to the system.

Effect of post-deformation annealing

HPT followed by post-deformation annealing (PDA) has been proposed to overcome the strength-ductility tradeoff typically observed in the heterogeneous microstructures of HPT hybrids [42,53]. This section presents the major microstructural evolutions reported in the hybrid systems (i.e. Zn-Mg and Al-Mg) subjected to PDA after HPT processing. The effects of the newly-formed microstructures after PDA on the micro-mechanical behaviour are covered in detail in "Nanoscale plastic deformation and strainrate sensitivity of HPT hybrids".

The significance of PDA was demonstrated by Valiev et al. [121] to improve both the tensile strength and elongation-to-failure of nanostructured Ti after HPT. According to a later review [122], the reason why PDA is an effective strategy to improve the overall ductility of a material is associated with an ordering of the defect structures within the grain boundaries, resulting in a near-equilibrium state without significant grain growth. In addition, PDA was found to reduce the dislocation density in the grain interiors of the UFG materials, giving an opportunity to increase the dislocation storage capability during plastic deformation, which may lead to enhanced ductility.

The influence of PDA in HPT hybrids was first investigated by Han et al. [42] for the Al-Mg system. They subjected a set of samples processed by HPT for 20 turns to a PDA treatment of 300°C for 1 h. The PDA-treated samples' microstructure was graded, where the central region contained a multilayered structure that was not present before PDA. Analysis of the disk edge revealed that the PDA-treated material exhibited a uniform equiaxed microstructure with a $GS_{ave} \sim 380 \text{ nm}$ containing $Al_{12}Mg_{17}$ and Al₃Mg₂ intermetallics and an Al-7Mg (at. %) solid solution phase. It is noted that before PDA, the HPT

samples also exhibited Al₁₂Mg₁₇ intermetallics. Therefore, it was evident that processing by HPT for 20 turns followed by PDA promoted the formation of a multicomponent Al-Mg hybrid system, which resulted in a simultaneous increase of the RT strain rate sensitivity and plasticity while maintaining a reasonable hardness.

Inspired by the latter example, the effect of PDA was recently studied by Hernández-Escobar et al. [53] on the Zn-Mg hybrid system by performing a 200°C/1 h PDA treatment to a set of HPT-processed samples for 30 turns. Experimental results indicated a microstructural evolution from a relatively equiaxed UFG structure with a GS range of 100-200 nm and Mg₂Zn₁₁ and MgZn₂ intermetallic nanoprecipitates evenly distributed after HPT, see Figure 9(a), to a heterogeneous microstructure with a bimodal GS distribution of $\sim 100-200 \text{ nm}$ and $\sim 600-900 \text{ nm}$ after PDA (Figure 9(b)). This was suggested to be a result of the segregation of the Mg₂Zn₁₁ and MgZn₂ nanoprecipitates in the Mg-rich grains, which may act as pinning sites preventing their grain growth during annealing. From the XRD analysis, it was found that PDA resulted in an increase of the Mg₂Zn₁₁ volume fraction at the expense of the MgZn₂ volume fraction, and this was associated with a decrease in the formation enthalpy, providing a lower energy state for the HPT hybrid system. Consistent with this, the formation of stable MgZn₂ nanosized precipitates in GP zones and grain boundaries was also reported in a recent work [123] investigating an HPT-processed Al-Zn-Mg-Zr alloy subjected to PDA between 120 and 170°C for 2 h. Like the Al-Mg hybrid system above, the microstructural evolutions that occurred in the Zn-Mg hybrid system after PDA led to a simultaneous increase in hardness and strain rate sensitivity.

Formation of supersaturated solid solutions

The extension of solid solubility in miscible metal systems, as well as the supersaturation of immiscible elements, have been demonstrated in numerous studies by the application of HPT [48,68,132,124-131]. This section presents, through several examples, a summary of the critical factors for HPT-induced supersaturation in hybrid systems, which is mainly influenced by the lattice structures, the heat of mixing, and the deformation behaviour.

Different combinations of lattice structures have exhibited supersaturation as a result of HPT processing, including FCC-FCC systems (Cu-Ag [124], Ni-Ag [125]), FCC-BCC systems (Cu-W [126], Cu-Cr [127,128], Cu-Fe [129,130], Cu-Ta [48]) and FCC-HCP systems (Cu-Co [131,133], Al-Mg [68,132]). The differences in lattice parameters and favourable slip systems between dissimilar lattice structures are

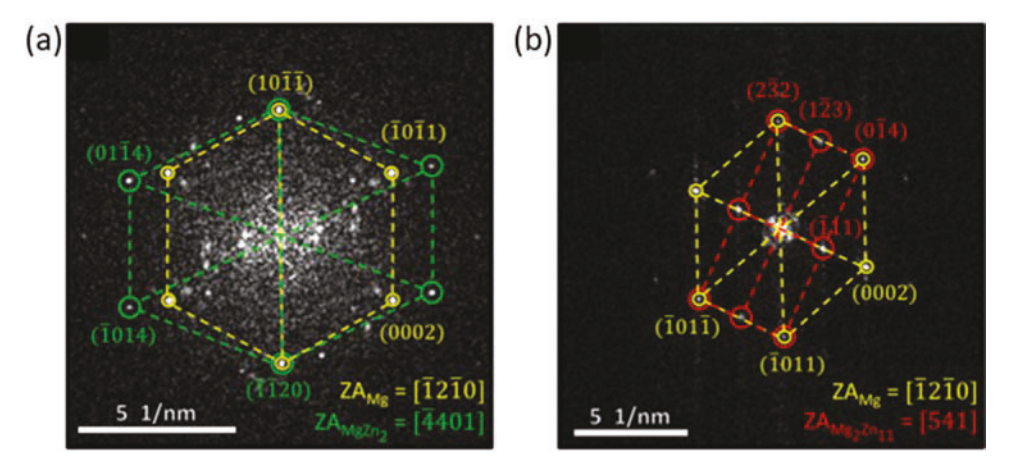


Figure 8. Intermetallic compounds (a) MgZn₂ and (b) Mg₂Zn₁₁ identified via FFT analysis of HRTEM images in the Mg-rich nanosized grain of the Zn-Mg HPT hybrids after 30 turns. Reproduced with permission from [53].

proposed to have an effect on the solubility limit, as they determine the dislocation glide across phase interfaces, which accounts for the dissolution of the constituent phases. The immiscible Cu-Co HPT hybrid system, obtained from powder consolidation, exhibited a maximum solubility of ~ 26 (at. %) Co in the Cu matrix, with a GS_{ave} below 50 nm [133]. In the Al-Mg system, a SSSS with a maximum solubility of ~ 39 (at. %) Mg in the Al lattice, having a

 $GS_{ave} \sim 35-40$ nm, was obtained after HPT processing for 100 turns using the multilayered approach sketched in Figure 3(d) [132]. Both of these studies revealed that, despite the original FCC-HCP nature of their hybrid systems, the SSSS developed after HPT exhibited a single FCC lattice. This implies that severe torsional straining can induce a phase transformation from HCP-to-FCC in Co and Mg, which was demonstrated experimentally for Co [134], and

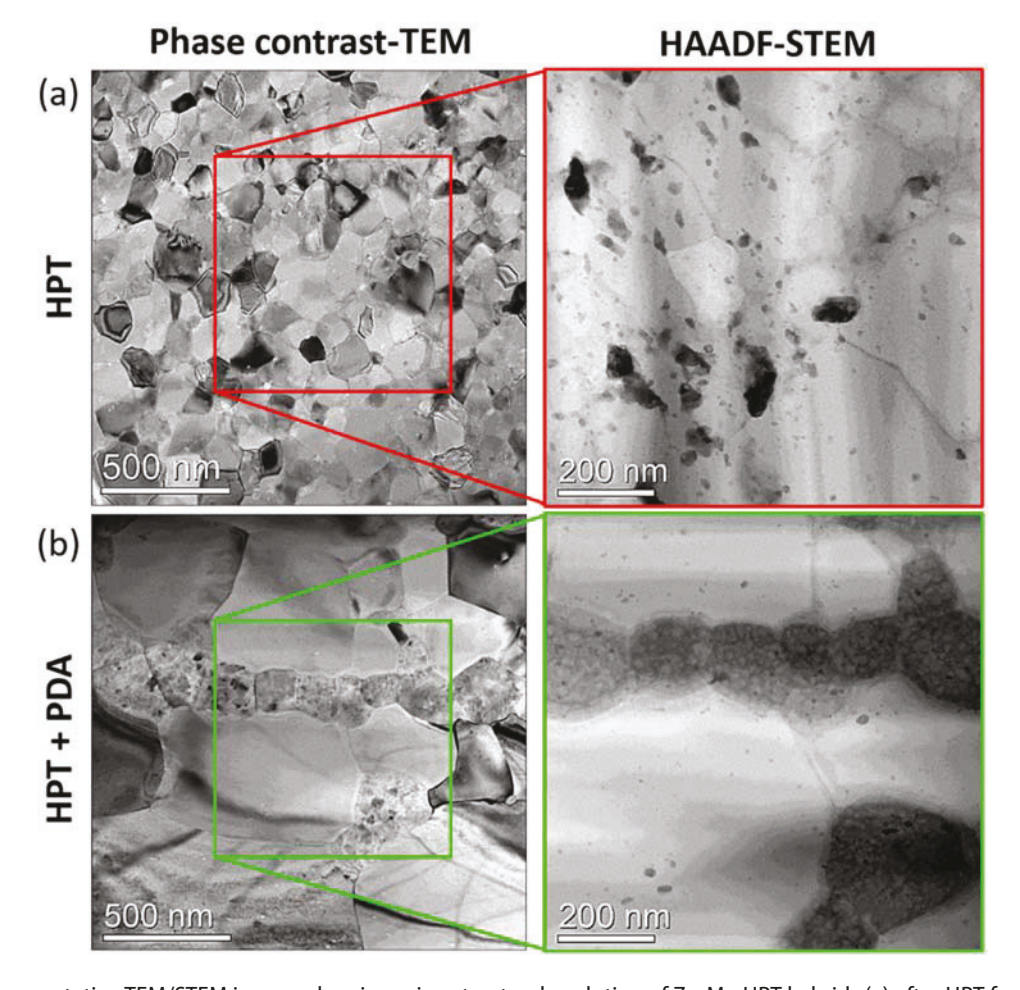


Figure 9. Representative TEM/STEM images showing microstructural evolution of Zn-Mg HPT hybrids (a) after HPT for 30 turns and (b) after additional PDA treatment (200 C for 1 h). Note that the image contrast in high-angle annular dark-field (HAADF) mode is proportional to the atomic number (i.e. brighter indicates a higher atomic number). Reproduced with permission from [53].

predicted from atomistic simulations for Mg [135,136]. Consistent with these studies, a recent work [137] reported the formation of a SSSS in the immiscible Mg-Hf system, as well as a HCP-to-FCC phase transformation after HPT processing.

On the other hand, the FCC-BCC hybrid systems after HPT exhibited comparatively lower solubility limits: ~ 20 (at. %) Fe, ~ 16 (at. %) Ta, ~ 5 (at. %) W and \sim 2 (at. %) Cr in the Cu lattice for the Cu-Fe [129], Cu-Ta [48], Cu-W [126] and Cu-Cr [128] systems, respectively. However, unlike the HCP materials in the FCC-HCP hybrid systems, all the BCC materials in these FCC-BCC hybrid systems were found to maintain their lattice structure upon supersaturation, thus, showing a mixture of FCC and BCC phases after HPT processing. It is worthwhile mentioning that BCC-to-FCC phase transformations are indeed possible in Fe [138], Ta [139], W [140], and Cr [141]; nevertheless, none of these were observed in the FCC-BCC hybrid systems after HPT. The apparent opposite trends followed by HCP and BCC metals, in terms of phase transformations, when combined with FCC metals can be understood from a maximisation of the number of deformation modes. Thereby, during HPT processing, HCP-to-FCC transformations are favourable as they involve an increase in the total number of slip systems from 3 to 12, whereas BCCto-FCC transformations are not favourable as they involve a decrease in the total number of slip systems from 48 to 12. Consequently, the presence of different lattice structures might have a detrimental effect on the compositional mixing and solid solubility required in the supersaturation process.

The enthalpy of mixing (ΔH_{mix}), also known as the heat of mixing, between different phases may also influence the formation of a SSSS in HPT hybrids. From the binary systems introduced in the previous paragraph, Kormout et al. [142] noted that the Cu-W system exhibited the largest ΔH_{mix} value, as well as the lowest solubility limit, and this trend was followed for the Ni-Ag and Cu-Cr systems. It may seem intuitive that the higher the ΔH_{mix} value (i.e. energy that the system requires to mix both elements), the more difficult it would be for both elements to mix, thereby favouring the formation of a SSSS. However, other systems like Cu-Fe, Cu-Co, and Cu-Ag did not follow that trend. It is, therefore, speculated that HPT processing might itself provide sufficient energy to overcome this thermodynamically unfavourable process in such a way that a low ΔH_{mix} value may not be an indicator for the formation of a SSSS during HPT processing.

Lastly, the deformation process, which in turn determines the strength differences between the phases forming the hybrid systems, has also been proposed to influence the degree of supersaturation in immiscible systems [142]. In the case of hybrids with a notable hardness difference between their constituent phases, plastic deformation is mainly carried by the soft phase, whereas fragmentation of the hard phase is expected, leading to microstructures based on partially supersaturated nanoscale phases or a fully supersaturated single-phase. Instead, when the hardness difference between phases is not significant, co-deformation of the individual phases is expected to create a lamellar structure. This leads to the formation of a SSSS if one of the phases is present in a much larger volume fraction or a micronanoscale phases structure of with supersaturation when the phase volume fractions are similar.

Other microstructural transformations in HPTprocessed hybrids

In addition to the nucleation of intermetallic compounds and the formation of metastable SSSS involhigh-pressure allotropic transformations presented in previous sections, the synthesis of HPT hybrids has shown additional microstructural features of interest, some of which are presented in this section.

At the nanometre level, the formation of amorphous phases and metastable solid solutions are competing processes during severe plastic deformation (SPD), where the microstructural stability of bulk nanostructured metals can lead to multiple scenarios [143]. A crystalline-to-amorphous transition, also referred as amorphisation, has been reported in some HPT-processed systems with negative $\Delta H_{\rm mix}$, but is not expected to take place in systems with positive ΔH_{mix} [144-146]. For instance, the formation of amorphous phases was recently observed in a V-alloy/Zr-alloy multilayered nanocomposite synthesised by HPT for 5 turns [147]. Ordered phases, including intermetallic compounds, have also been found to undergo amorphisation, as is the case of the Ni₃Al intermetallic compound, which transforms into disordered nanocrystalline phases during HPT processing [148]. The presence of intermetallic compounds seems to be critical for the microstructural stability of the SSSS during HPT. Despite their positive ΔH_{mix} , systems that do not form intermetallic compounds, like Al-Zn, Cu-Co, Cu-Ni, and Cu-Ag systems, decomposed during HPT processing [119,149,150].

The thermal stability of SSSS synthesised by HPT has been examined in multiple works [48,126,128,129,131,151], and it has been generally found to be significantly higher than expected both in single-phase and multi-phase microstructures [143]. Decomposition is typically reported at low annealing temperatures, such that phase separation takes place before grain growth. This enables the formation of immiscible UFG composites that considerably slow down the kinetics for grain growth through boundary migration. It was further shown that the decomposition of SSSS could lead to the formation of bulk metallic glasses during HPT, as it was reported for a wide range of compositions in the Cu-Zr and Cu-Zr-Al systems [152]. However, the presence of intermetallic compounds, even in systems with negative ΔH_{mix} , like the Cu-In system, seems to be critical for maintaining the SSSS during HPT processing [153].

Despite the increased scientific interest in heterostructured materials and the number of publications highlighting the potential of HPT for their synthesis, until recently, little was known regarding the comparative attributes of HPT-processed hybrids with respect to a homogenous material having equivalent nominal composition. The work of Hernández-Escobar et al. [54] provided the first study to directly compare the microstructure and the hardness evolution between a Zn-3Mg (wt. %) alloy and its hybrid counterpart, after high-pressure torsion (HPT), and after HPT followed by a post-deformation annealing (PDA) treatment. Experimental results indicated that both the alloy and the hybrid reached a similar level of grain refinement after HPT processing; however, grain growth followed different trends after PDA. The HPT-processed alloy exhibited clusters of Mg₂-Zn₁₁ nanocrystalline domains that coalesce into coarser grains, maintaining a unimodal GS distribution after PDA. On the contrary, the hybrid after PDA displayed a multimodal GS distribution consisting of ultrafine Mg-rich grains containing MgZn₂ and Mg₂- Zn_{11} nanoscale intermetallics in a matrix of coarser dislocation-free Zn grains. To the authors' knowledge, there is not any additional study to date exploring the comparative microstructural characteristics and micromechanical behaviour between an HPT alloy and its hybrid counterpart.

Micro-mechanical properties of HPTprocessed metal hybrids

Hardening mechanisms of HPT hybrids obtained from mechanical bonding

The extraordinary grain refinement and the development of microstructural transformations, including the nucleation of intermetallic compounds and the formation of SSSS of the HPT-processed hybrids, lead to significant hardness increases. Hardness measurements are typically recorded from the crosssection of the disk sample along its diameter, either linearly at the mid-thickness plane (1D) along the radial direction, or through a rectilinear grid pattern (2D) across both the radial and thickness directions. This section presents the evolution of HV values for different HPT hybrid systems at increasing number of turns, discusses the strengthening mechanisms involved in such evolutions, and compares the HV

values obtained from HPT hybrids with those reported from other SPD processes. It should be emphasised that the HV values presented in this section are obtained from microscopic indentations (typically 10–200 μm [154]), which correspond to limited local microstructural patches. Therefore, whereas the evolution of HV values during different processing conditions can be correlated with microstructural evolutions, they should not be used to infer global mechanical properties like strength or elongation-tofailure from the bulk material.

The HV evolution of Al-Cu hybrids processed by HPT for 10, 20, 40, and 60 turns, whose cross-sections are depicted in Figure 4(a), is presented along the disk diameters in Figure 10(a) [39]. For comparison, the HV values for Al and Cu processed separately by HPT for 10 turns are denoted by dashed lines at \sim 65 and \sim 150 HV, respectively. The central regions of the disk after 10 turns at $r \lesssim 4$ mm, after 20 turns at $r \lesssim 2$ mm, and after 40 turns at $r \lesssim 1$ mm, show similar hardness values, which are slightly lower than 150 HV. In contrast, the hardness at peripheral regions of the disks after 10, 20-40, and 60 turns reach maximum values of ~ 250, ~ 400, and ~ 500 HV, respectively. This increasing hardness trend was consistent with the presence of Al₂Cu, AlCu, and Al₄Cu₉ intermetallic compounds near the disk edges after 20 turns and their higher volume fractions at increasing numbers of turns [39]. For comparison, the microhardness of a multilayered Al-Cu composite produced by ARB reached ~ 160 HV in the Cu-rich region, and ~ 80 HV in the Al-rich region after 2 cycles [155]. In a separate ARB-processed Al-Cu hybrid, the microhardness was reported to increase from 21 to 134 HV in the Al layers, and from 53 to 168 HV in the Cu layers after 8 cycles [156]. On the other hand, ECAP-processed Al-Cu alloys containing 2-5 (wt. %) Cu reached microhardness values ranging from ~ 140 to 200 HV after 8 passes, with increasing microhardness at increasing Cu content [157,158]. It should be noted that no intermetallic compound formation was reported in the Al-Cu system after ARB or ECAP processing, which is likely the reason why these SPD techniques tended to exhibit lower HV values compared to those obtained from HPT.

The HV values recorded along the disk diameter of the HPT-processed Al-Mg hybrids after 1, 5, 10, 20, 40, and 60 turns, corresponding to the cross-sections observed in Figure 4(b), are presented in Figure 10 (b) [70]. For reference, the saturation HV values reported for Al-1050 [159] and ZK60 [160] alloys after 5 turns are marked with dashed lines at ~ 65 and ~ 110 HV, respectively. At least 10 turns were needed in order to obtain HV values significantly higher than those within the range defined by the reference dashed lines, and these were found at $r \gtrsim$

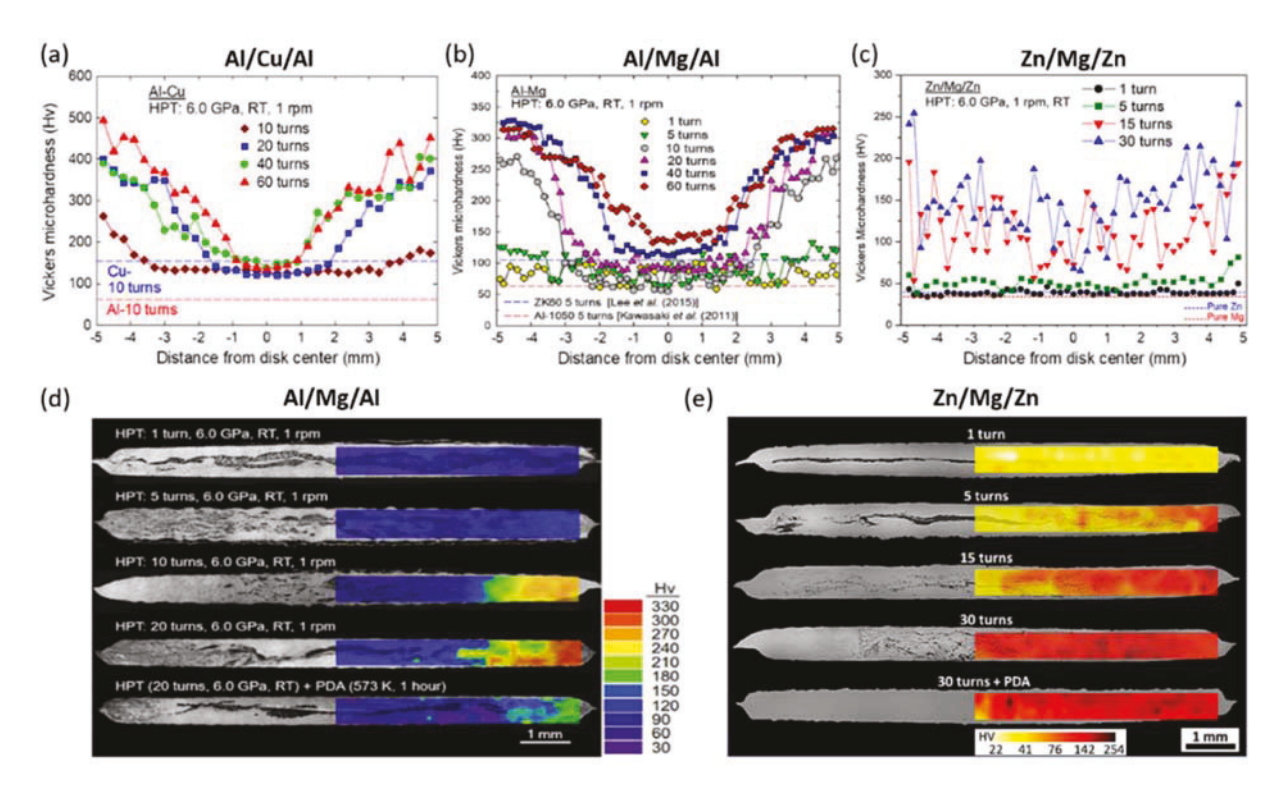


Figure 10. Vickers microhardness (HV) evolution across the diameter at the mid-thickness plane of the (a) Al-Cu HPT hybrid system, (b) Al-Mg HPT hybrid system, and (c) Zn-Mg HPT hybrid system; Colour-coded HV contour plots of the (d) Al-Mg HPT hybrid system and (e) Zn-Mg HPT hybrid system overlapped on top of their corresponding SEM cross-sections. Reproduced with permission from [39,43,46,52,53].

3 mm. After 20 turns, a saturation hardness value of 330 HV was found close to the disk periphery, $r \gtrsim$ 4 mm, and it was relatively uniform up to 60 turns. A gradual hardness increase at the central disk region, -2 < r < 2 mm, to ~ 115 and ~ 140 HV was reported with increasing number of turns to 40 and 60, respectively. Note the lack of radial symmetry in the hardness distribution after 60 turns, which was associated with the misalignment of the HPT anvils during long-time processing. However, the hardness values reported with and without misalignment were found to be consistent with a separate study [161], except for the shifting of the central region. Figure 10(d) shows a series of colour-coded contour maps of the HV overlapped on the cross-sections of the Al-Mg HPT hybrids from 1 to 20 and 20 turns + PDA (300°C, 1 h) [42]. PDA resulted in a hardness decrease, from \sim 60 to \sim 30 HV in the central regions, -3 < r < 3 mm, and from ~ 330 to ~ 220 HV at the disk periphery, $r \gtrsim$ 4 mm. This softening was attributed to the increase of the GS_{ave} from ~ 60 to ~ 380 nm and the dissolution of the Al₁₂Mg₁₇ intermetallic as a result of the PDA treatment [42].

For comparison, the microhardness of an Al-Mg laminated composite fabricated by ARB saturated at $\sim 100~\rm HV$ in the Al-rich layers, and at $\sim 50~\rm HV$ in the Mg-rich layers after 2 cycles [162]. These results were consistent with those reported from an ARB-processed Al-AZ31 multilayered hybrid in a different

work [163]. It should be noted that intermetallic compounds, namely Al₃Mg₂ and Al₁₂Mg₁₇, with ~ 200 HV, were identified at the interface between Al layers and Mg layers after 3 cycles, which led to obvious cracking and premature failure during tensile testing [162,164]. On the other hand, Al-2.77Mg (wt. %) cast alloy subjected to ECAP showed an increase in microhardness from ~ 450 HV to ~ 750 , 850, and 900 HV after 1, 2, and 4 passes, respectively [165]. Upon applying a PDA treatment (i.e. 250°C for 90 min) to the ECAP-processed samples, their microhardness decreased to ~ 550 HV after 1 pass and saturated at ~ 600 HV after 2 passes [165]. This softening is consistent with the decrease in microhardness reported above from Al-Mg HPT hybrids after PDA, and might be due to the dissolution of intermetallic compounds during PDA. It should be noted that the latter HV values are significantly larger than those above for Al-Mg HPT hybrids. However, not only the number of ECAP passes plays a role in hardness increase, but also other factors like the material texture or the Al content of the alloy, which is notably greater in the latter ECAP-processed samples. For instance, in an AZ31 alloy, which only contains 3 (wt. %) Mg, the microhardness just increased from 65 HV to 76, 78, 83, and 85 HV after ECAP for 1, 2, 4, and 8 passes, respectively [166]. This evidences that it is not possible to compare the effect of different SPD methods on the mechanical properties unless the starting materials

have an equivalent nominal composition and processing history.

The distribution of HV values at the mid-thickness plane of the Zn-Mg HPT hybrids after 1, 5, 15, and 30 turns, corresponding to the cross-sections observed in Figure 4(c), is depicted in Figure 10(c) [52]. The HV values of pure Mg [167] and pure Zn [168], which are 35 and 37 HV, respectively, are provided for comparison. After 5 turns, a relatively uniform hardness of 50-70 HV was recorded across the sample, with a maximum of ~ 80 HV near the disk edge. Processing for 15 turns not only significantly increased the HV values, reaching a maximum of ~ 200 HV at the periphery, but also led to a wide Hv range ($\sim 70-180 \text{ HV}$) across the disk diameter. The same trend was observed after 30 turns, where a maximum of $\sim 250 \, \text{HV}$ was found at the disk edge, and a wide range of hardness values (between 70-200 HV) was measured across the sample. Both the notable increase of HV values and the hardness heterogeneity after 15 and 30 turns were associated with a notable decrease of the GS_{ave}, as well as the nucleation of heterogeneously dispersed nanoscale Mg₂Zn₁₁ and MgZn₂ intermetallics, whose volume fractions increased with the number of turns. The effect of post-deformation annealing (PDA) on the hardness evolution of the Zn-Mg hybrid after HPT for 30 turns can be observed in Figure 10(e), which shows a series of colour-contour maps corresponding to hybrids with a nominal composition of Zn-3Mg (wt. %) processed under the same conditions than those in Figure 4(c) [53]. The HV values followed a symmetric gradient-type evolution with respect to the centre from 1 to 30 turns, having maximum values

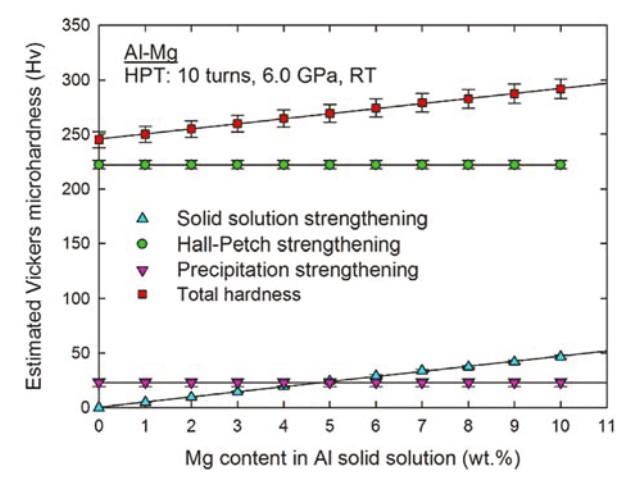


Figure 11. Estimated Vickers microhardness (HV) values for increasing Mg content in Al solid solution in Al-Mg HPT hybrids after 10 turns; the estimated total hardness is denoted by the red squares with error bars, and the hardness of the three different strengthening mechanisms of solid-solution strengthening, Hall-Petch strengthening, and precipitation strengthening are denoted by blue upright triangles, green circles, and pink inverted triangles with error bars, respectively. Reproduced with permission from [68].

within the range of 200-230 HV. Unlike the Al-Mg HPT hybrid system above, the Zn-Mg hybrid did not exhibit softening after PDA, but instead presented maximum hardness values in the range of 210-250 HV, which were the highest hardness values recorded for the Zn-Mg HPT hybrid system. For comparison, a Zn-3Mg (wt. %) alloy subjected to ECAP increased its average microhardness from 175 HV to 180 and 186 HV after 1 and 2 passes, respectively [169]. It should be noted that the nominal composition of this ECAP-processed sample is equivalent to that of the Zn-Mg HPT hybrids [53], where hardness values in the range of 210-250 HV were reported at the disk periphery after 30 turns. To the authors' knowledge, these works [53,169] are the only ones currently available in the literature that report the microhardness values of Zn-Mg materials processed by SPD methods.

An investigation of the different mechanisms responsible for the strain hardening in the HPT hybrids was presented in an earlier work by Ahn et al. [68] for the Al-Mg system. The total hardness increase was assessed through the combination of three mechanisms: (1) Hall-Petch strengthening associated with the significant grain refinement, (2) precipitation strengthening associated with the nucleation of Al₃Mg₂ and Al₁₂Mg₁₇ intermetallic compounds, and (3) solid-solution strengthening due to the accelerated diffusivity of Mg into Al-rich phases. The experimental parameters required for the equation models proposed (i.e. grain sizes, phase fractions, grain boundary fractions, etc.) were directly obtained from TEM and XRD analysis of the Al-Mg HPT hybrids, whereas some constant values (i.e. Burgers vectors, activation energies, diffusion coefficients, etc.) were obtained from Al-Mg alloys in the literature. The contribution of each of the three strengthening mechanisms to the total hardness of the Al-Mg hybrids after HPT for 10 turns can be observed in Figure 11 for different Mg contents in Al solid solution. The hardness model was consistent with the experimental HV values. For example, for a 5 (wt-%) Mg in Al, the model predicted $\sim 269 \pm 8$ HV, which is in good agreement with the experimental value at the periphery after 10 turns, as observed in Figure 10(b). It is interesting to note these authors left out strain hardening due to dislocation impingement/ entangling, yet it is likely that this strengthening mechanism was also active.

Given the success of the hardening model presented, it may seem trivial to expand it to other HPT hybrid systems. However, the contributions of the three strengthening mechanisms considered above are closely related to the microstructural evolution of each system and may be completely different from one material to another. Moreover, additional strengthening mechanisms, which have been

identified to play a relevant role in metal-matrix composites, like (1) the load transfer effect and (2) the coefficient of thermal expansion (CTE) and Youngs modulus (E) mismatch effect [170-173], may also take place in the HPT hybrids. For instance, the load transfer effect, which occurs between the soft/compliant matrix and the stiff/hard reinforcement under an applied external load, may occur in those hybrid systems where intermetallic compounds were found dispersed in the matrix. Nevertheless, the contribution of the load transfer effect to the total strength may not be significant unless the volume fraction of intermetallic phases is large enough and/or the aspect ratio of the reinforcement is above a certain value [172]. Similarly, the CTE or the E mismatch between the matrix and the reinforcement can produce additional stresses under an applied load, thereby increasing the content of geometrically necessary dislocations at the matrixreinforcement interface [170]. The CTE mismatch effect may not be relevant to the total strength, provided that there were no sudden temperature changes during processing, as was the case of the HPT hybrids synthesised at room temperature (RT). However, the CTE mismatch effect was reported to become even more significant than Orowan strengthening in metal-matrix composites obtained at high temperatures (i.e. ~ 300°C) [170]. It was also noted that grain boundary sliding is another deformation mechanism that may be active in HPT-processed materials, yet it was not mentioned in the above studies, and it is discussed in "Nanoscale plastic deformation and strain-rate sensitivity of HPT hybrids". Overall, further investigations that account for all possible deformation mechanisms are needed in order to develop a thorough understanding of the underlying strengthening mechanisms for different hybrid systems processed by HPT.

Evaluation of global mechanical properties from HPT hybrids

The small dimensions of conventional HPT samples ($\sim 10 \text{ mm}$ diameter and $\sim 1 \text{ mm}$ thickness) limit the evaluation of their mechanical properties beyond microhardness using standard testing geometries and procedures. However, several works have reported stress-strain curves from uniaxial tensile testing [174-180], as well as stress vs. number of cycles to failure curves [181-183] or crack growth curves [184-186] from fatigue testing using specimens taken from HPT-processed pure metals and alloys. Global mechanical properties, including ultimate tensile strength (UTS), yield strength (YS), and elongation-to-failure (ε_f), have also been reported from different HPT-processed hybrids. For example, Al-matrix composites reinforced with 0.25-0.5 (wt. %) graphene platelets synthesised by HPT exhibited an enhanced UTS and microhardness, up to ~ 200 MPa and ~ 120 HV, compared with pure Al and Al-matrix composite reinforced with C nanotubes subjected to HPT, while maintaining a reasonable ε_f [93]. In a separate work, a set of Cu-NbC hybrids with 0.5-5 (vol. %) NbC fabricated from powder consolidation using HPT followed by shorttime annealing at 600-700°C, exhibited increased UTS and microhardness as a function of the NbC fraction, up to ~ 1 GPa and ~ 250 HV, respectively [187]. Another set of powder-consolidated Al-10Fe (wt. %) hybrids via HPT up to 75 turns exhibited different combinations of UTS and ε_f , ranging from 100-500 MPa and 10-55%, respectively, and showed interesting strength-ductility combinations at intermediate levels of imposed strain [83]. Nevertheless, the stress-strain behaviours above 50 turns were found to be inconsistent between different tensile specimens extracted from the same sample. Such inconsistencies were attributed to the heterogeneous distributions of the dissolved Fe solute atoms into the Al matrix leading to heterogeneous hardness distributions within the test gauges prepared after such high deformation by HPT [83].

To the best of the authors' knowledge, only the recent work from Bazarnik et al. [188] has presented stress-strain data from miniature tensile testing of HPT-processed hybrids using the multilayer format shown in Figure 3(d). The authors [188] synthesised Al-Cu HPT hybrids for 20, 50, 150, and 200 turns and measured UTS values of 420, 460, 710, and 910 MPa, respectively. Nevertheless, these hybrid materials exhibited a limited ε_f of $\sim 2\%$. This pioneering work enabled a direct correlation between macroand micro-mechanical properties in multilayered HPT hybrids through the comparison of stress-strain data and microhardness data across the HPT disk.

The fact that the later work was not overly promising in terms of achieving an adequate strength-ductility combination from Al-Cu HPT hybrids should not discourage the study of global mechanical properties at the macroscale, such that these can be coupled with micro- and nano-mechanical data for a deeper understanding of the processing-microstructureproperty relationships of HPT hybrids. Furthermore, current and future researchers in this field are strongly encouraged to investigate the mechanical properties at different scales (i.e. macro- (tensile testing), micro-(microhardness), and nano- (nanoindentation)) to better assess the effect of the microstructural evolutions in the HPT hybrids. Such studies would enable a significant contribution to the development of heterostructured nanocrystalline metals [8]. This is also expected to help clarify the fundamentals behind the strength-ductility synergy reported in several HPT hybrids, as well as to enable a comprehensive comparison of the global mechanical properties (i.e. UTS, YS, ε_f) between HPT and other deformation methods, which unfortunately is not possible today.

Nanoscale plastic deformation and strain-rate sensitivity of HPT hybrids

To date, the research interest in HPT hybrids has been mainly focused on identifying the mechanisms of the metal mixture and bonding, as well as the strengthening mechanisms at the microscale and the nanoscale. Considering the inherent microstructural heterogeneity across the HPT hybrids, nanoindentation has been deemed to be a versatile technique for testing local mechanical properties (beyond hardness (H) and Young's modulus (E)). Unlike tensile or fatigue testing, the use of nanoindentation enables the investigation of the plastic deformation behaviour in small volumes of the sample. The versatility of nanoindentation testing allows the design of test protocols capable of determining microstructure-dependent parameters like the strain rate sensitivity (m) and the activation

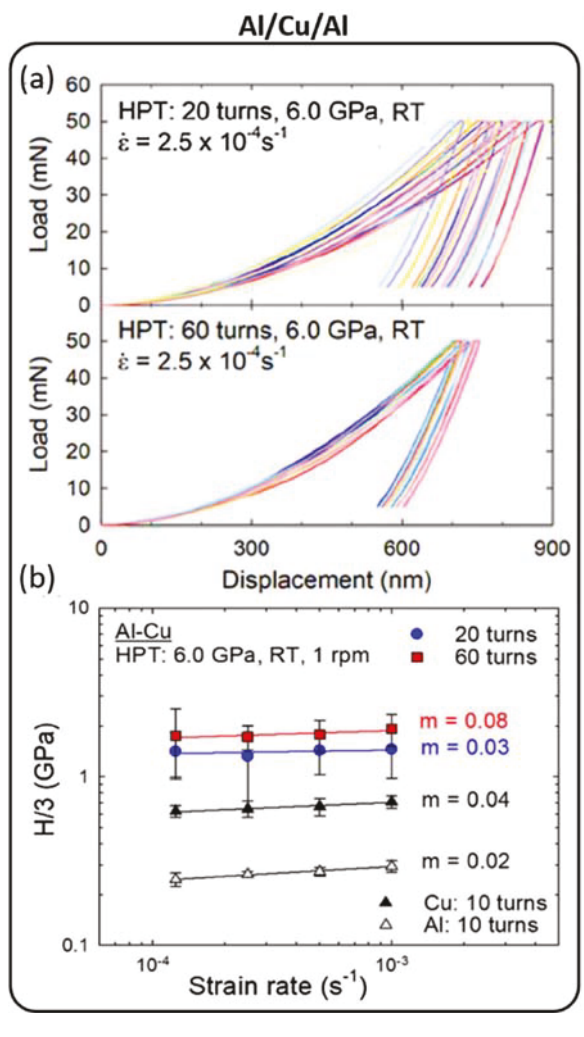


Figure 12. (a) Load-displacement curves obtained from nanoindentation at $\dot{\epsilon}=2.5\cdot 10^{-4}~\text{s}^{-1}$ at the edge of the Al-Cu HPT hybrids after HPT for 20 and 60 turns, and (b) logarithmic plot of H/3 vs. $\dot{\epsilon}$ showing the corresponding m values, which are compared to those of pure Cu and Al after HPT for 10 turns. Reproduced with permission from [43].

volume (V^*) , which provide insights related to the underlying deformation mechanisms. This section presents a series of studies where nanoindentation testing was performed under different conditions on multiple HPT hybrids, and it was used to reveal critical information about their plastic deformation behaviour at the nanoscale.

Plastic instability in HPT hybrids results from microstructural heterogeneity (i.e. inhomogeneous distributions of grain sizes and phases), and this is manifested through a relative deviation between load-displacement curves obtained from different nanoindentations within the same local area. This phenomenon can be observed in a series of separate load-displacement curves obtained under an applied load of 50 mN and an equivalent strain rate (έ) of $2.5 \cdot 10^{-4} \, \text{s}^{-1}$ at the disk edges of the Al-Cu HPT hybrids after 20 and 60 turns [43], shown in Figure 12(a). Increasing the number of turns from 20 to 60 resulted in a significant decrease of plastic instability, as the broadening between different load-displacement curves was greatly reduced. This was attributed an enhanced microstructural uniformity at increased torsional straining, which also led to a higher H as a result of the increased content of intermetallic phases and extreme grain size refinement, as observed by the lower displacement values after 60 turns. Load-displacement curves recorded at different $\dot{\epsilon}$ were then used to obtain the m values using Tabors empirical relationship [189], which are plotted in Figure 12(b) in comparison with those of commercially pure Cu and Al processed separately by HPT for 10 turns. It was found that both the *H* and *m* values corresponding to the Al-Cu hybrids are higher than those of Al and Cu HPT-processed separately. In addition, both the H and m values increased for the Al-Cu HPT hybrids with increasing number of turns. The increase in m from 20 to 60 turns was associated with the configurational transformation from a layered nanostructure after 20 turns into an equiaxed nanostructure after 60 turns, which was expected to enhance grain boundary sliding activity, thus providing potential for achieving enhanced plasticity.

The effect of the nanoindentation strain rate on the mechanical response of the HPT hybrids was first investigated in the Al-Mg system [45]. Figure 13(a) shows a series of load-displacement curves recorded under an applied load of 50 mN at $\dot{\epsilon} = 1.25 \, 10^{-4}$, $2.5 \, 10^{-4}$, $5.0 \, 10^{-4}$ and $1.0 \, 10^{-3} \, s^{-1}$ at the disk edge ($r \approx 5$ mm) of the Al-Mg hybrids after HPT for 5 turns. Plastic instability becomes larger with increasing $\dot{\epsilon}$, as the broadening between load-displacement curves increases gradually from $1.25 \, 10^{-4}$ to $1.0 \, 10^{-3} \, s^{-1}$. It was also noted that the variability between different curves becomes narrower, as they shift slightly to the right at decreasing $\dot{\epsilon}$ values. Since

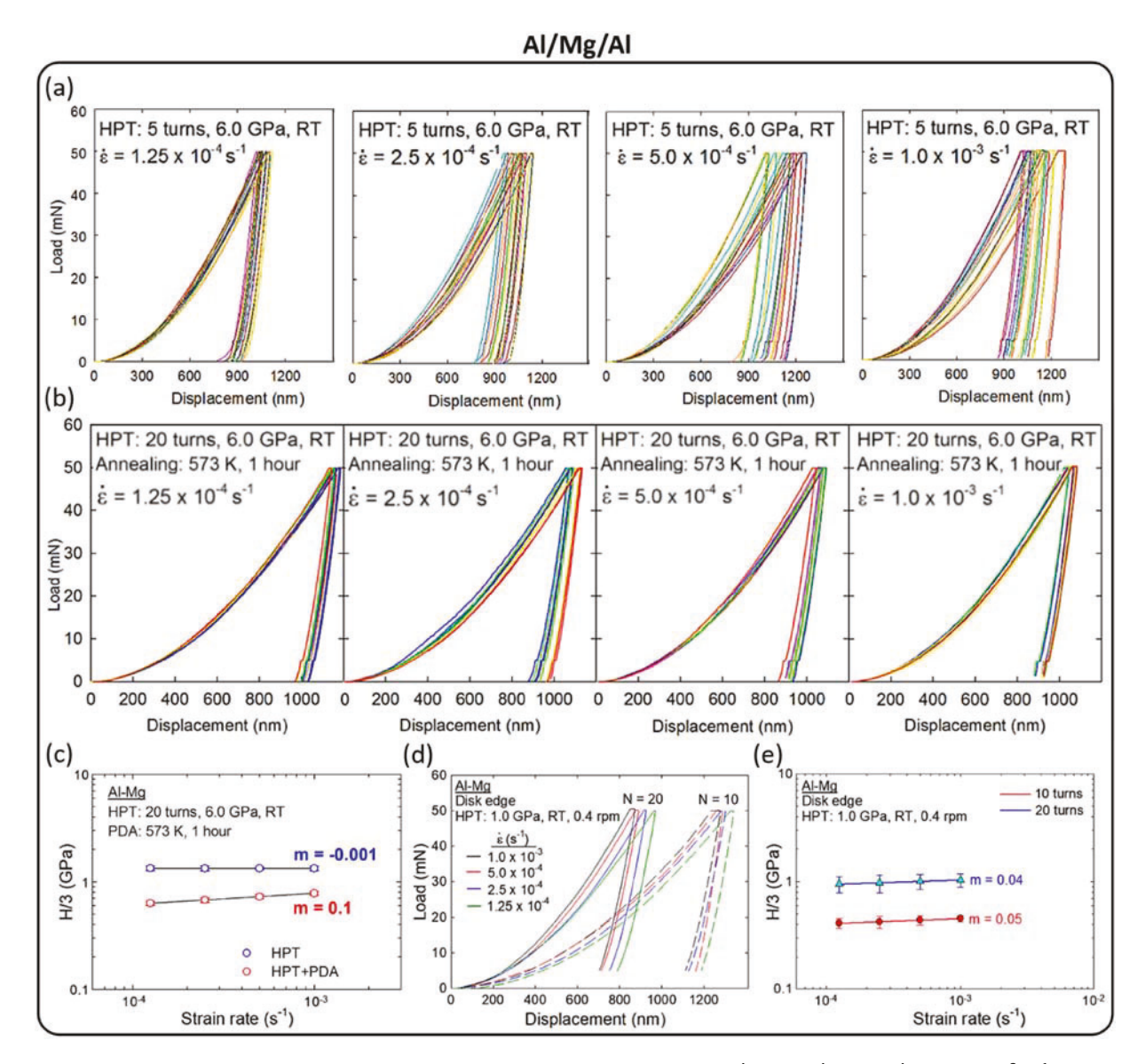


Figure 13. Load-displacement curves obtained from nanoindentation at = $1.25 \cdot 10^{-4}$, $2.5 \cdot 10^{-4}$, $5.0 \cdot 10^{-4}$ and $1.0 \cdot 10^{-3}$ s⁻¹ at the disk edge (r ≈ 5 mm) of the Al-Mg HPT hybrids after HPT for (a) 5 turns and (b) 20 turns + PDA (300 ? for 1h); (c) logarithmic plot of H/3 vs. showing the m values after HPT for 20 turns and 20 turns + PDA; (d) load-displacement curves at the same four different $\dot{\epsilon}$ values above and (e) corresponding logarithmic plot of H/3 vs. $\dot{\epsilon}$ showing the m values obtained at the disk edge (r ≈ 10 mm) of scaled-up Al-Mg hybrids having 25 mm diameter after HPT for 10 and 20 turns. Reproduced with permission from [42,44,45,47].

the final displacements at different ε values are fairly consistent, no strain rate dependency was reported on the Al-Mg hybrids after HPT processing for 5 turns [45], and the same was true after 20 turns [44]. The effect of post-deformation annealing (PDA) on the strain rate dependency was reported for Al-Mg hybrids processed by HPT for 20 turns + PDA (300° C, 1 h) at the same four $\dot{\epsilon}$ values mentioned above [44], and their corresponding load-displacement curves are presented in Figure 13(b). Unlike after HPT, the microstructural changes during PDA resulted in decreasing displacements at higher ἑ values, thereby indicating a strain rate dependency. It should be mentioned that for all strain rates, the Al-Mg hybrids after HPT exhibited lower displacements than after HPT + PDA, which is in agreement with the colour-coded HV contour maps in Figure 10(d). The corresponding softening of the Al-Mg system associated with the PDA can be observed in the logarithmic plot of H/3 vs. $\dot{\epsilon}$ depicted in Figure 13 (c) [42], where the positive slope after PDA denotes a positive m value (0.1). This demonstrates the feasibility of the PDA treatment for enhancing the plasticity of Al-Mg hybrids at RT without compromising the hardness significantly. The slightly negative m value (-0.001) reported after HPT might be associated with the Portenvin–Le Chatelier effect [190]; however, its close proximity to zero truly reflects the lack of strain rate dependency after HPT processing alone.

The influence of scaling up the conventional dimensions of the HPT samples (i.e. 10 mm diameter) on the micromechanical behaviour was evaluated using nanoindentation near the edge of the Al-Mg hybrids having 25 mm diameter after HPT processing

for 10 and 20 turns [47]. The significant hardness increase from 10 to 20 turns was evident from the decrease in the final displacement values, which can be observed in the load-displacement curves depicted in Figure 13(d), obtained under an applied load of 50 mN at the same 4 different $\dot{\epsilon}$ values mentioned in the previous paragraph. Unlike for the conventional Al-Mg hybrids after 5 and 20 turns, strain rate dependency of the plastic response was observed in the scaled-up versions after 10 and 20 turns, which in fact exhibit the same trend of faster \(\bar{\epsilon}\) values resulting in higher hardness values [47]. This trend, consistent with that of the conventional Al-Mg hybrids after 20 turns HPT + PDA (see Figure 13(b)), is responsible for the positive m values of 0.05 and 0.04 after 10 and 20 turns, respectively, which are reported in the H/3 vs. $\dot{\epsilon}$ plot in Figure 13(e). By comparing the conventional and scaled-up hybrids after 20 turns in the samples, in Figure 13(c,e), respectively, one can see a fairly consistent hardness value around 1 GPa in both cases. However, the conventional hybrid did not show any strain rate dependency, whereas the scaled-up sample did, resulting in a positive *m* value. This might be associated with an enhanced atomic mixing due to a larger sample volume, which led to a higher microstructural homogeneity, similar to the PDA effect on the conventional hybrids.

Following the studies performed in the Al-Mg hybrid system, the plastic behaviour of Zn-Mg hybrids under different conditions was examined through a series of nanoindentations located at the disk periphery under varying strain rates [53]. Representative load-displacement curves collected under an applied load of 50 mN at $\dot{\epsilon} = 1.25 \cdot 10^{-4}$, $2.5 \cdot 10^{-4}$, $5.0 \cdot 10^{-4}$ and 1.0 10⁻³ s⁻¹ are presented in Figure 14(a,b), for the sample after HPT for 30 and 30 turns + PDA (200°C, 1 h), respectively. Despite both samples exhibiting some broadening between separate measurements, which seemed to be independent of the $\dot{\epsilon}$ value, their average displacements decreased with increasing \(\bar{\epsilon}\). As a consequence of this trend, both material conditions exhibited a positive m value, as observed in Figure 14(c), which was slightly larger after PDA (0.121) than right after HPT for 30 turns (0.098). In addition, the average displacements after PDA were consistently lower than after HPT for 30 turns, and this was true for all the & values tested, indicating that the disk edges of the Zn-Mg hybrids became harder after the PDA treatment, contrary to what was reported in the Al-Mg hybrids.

The unusual mechanical response of the HPT-processed Zn-Mg hybrids after PDA was attributed to the formation of a bimodal grain size distribution, which in turn resulted from the segregation of intermetallic precipitates in Mg-rich grains, hindering their grain growth during annealing. To further investigate the origin of the synergistic effect of PDA on the mechanical behaviour of Zn-Mg HPT hybrids, the unloading stiffness (S) and the displacement at peak load (h_{max}) were obtained from the load-displacement curves [53]. Both S and h_{max} decreased after PDA. They also decreased with increasing $\dot{\epsilon}$ for each sample condition. The theoretical models presented in Figure 14(d,e) were proposed to illustrate the individual effects of S and h_{max} , respectively, in the load-displacement behaviour of two materials (1 and 2) with different hardness [53]. On the one hand, if $S_1 < S_2$, material 1 experiences a larger elastic recovery (i.e. lower plastic deformation) and thus, will be harder than material 2 (assuming same loading rates) (see Figure 14(d)). On the other hand, if $h_{\text{max}1} < h_{\text{max}2}$, material 1 requires a lower plastic strain to reach the peak load, and thus, it will be harder than material 2 (assuming same unloading rates) (see Figure 14(e)). In these models, material 1 (blue colour) represents the sample after HPT, and material 2 (red colour) represents the sample after HPT + PDA, in agreement with the colour selection across the figure. This work demonstrated that the parameters of the PDA treatment could be tailored to produce a dual enhancement of hardness and plastic deformation capability, which was associated to the presence of hard and soft domains playing complementary roles in the microstructure, thereby defying the classical strength-ductility tradeoff.

Towards strength-ductility synergy through heterogeneous microstructures

Ultrafine-grained (UFG) metals and alloys processed by techniques of severe plastic deformation (SPD) often experience high strength but limited ductility, which refers to the so-called paradox of strength and ductility [7,191,192]. The decrease of ductility (elongation-to-failure in uniaxial tension) in metals with nano- and submicron-sized grains is mainly associated with a reduction of the strain hardening capacity. As it is well known from the Hart's criterion [193], localised deformation leading to plastic instability sets in when Equation (4) below is fulfilled:

$$\frac{\partial \sigma}{\partial s} + m\sigma \le \sigma \tag{4}$$

where σ is the true stress, ε is the true strain, m is the strain rate sensitivity, and $\partial \sigma / \partial \varepsilon$ is the strain hardening rate, which reflects the strain hardening capability of a material. It is apparent that one should either increase the strain-hardening rate and/or the strain rate sensitivity to keep up with the increasing stress during plastic deformation for averting the condition in Equation (4) from being met. In general, UFG metals with homogenous microstructures (i.e. uniform grain sizes) exhibit a limited strain hardening capability as a result of a quick saturation of the

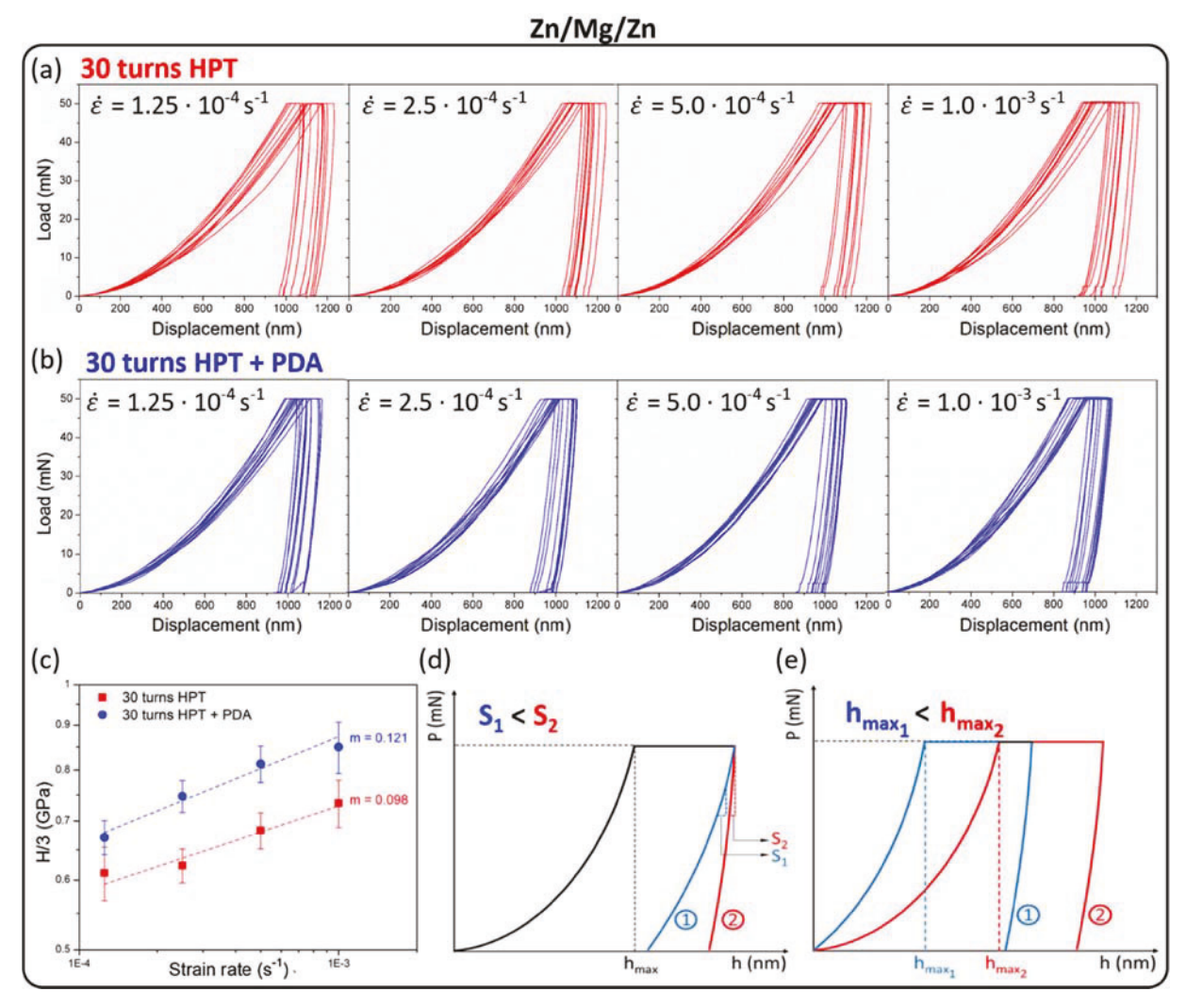


Figure 14. Load-displacement curves obtained from nanoindentation at $\dot{\epsilon} = 1.25 \cdot 10^{-4}$, $2.5 \cdot 10^{-4}$, $5.0 \cdot 10^{-4}$ and $1.0 \cdot 10^{-3}$ s⁻¹ at the disk edge (r \approx 5 mm) of the Zn-Mg HPT hybrids after HPT for (a) 30 turns and (b) 30 turns + PDA (200 °C for 1 h); (c) logarithmic plot of H/3 vs. $\dot{\epsilon}$ showing the m values after HPT for 30 and 30 turns + PDA; Theoretical load-displacement curves for two materials having (d) different S values and (e) different h_{max} values. Reproduced with permission from [53].

dislocation density due to dynamic recovery at room temperature (RT) during SPD [3]. Similarly, the strain rate sensitivity is often not sufficiently high (i.e. m ? 0.5 at RT) in SPD-processed materials, including HPT-processed metals, as it is inversely proportional to the strength level [194]. In this regard, heterogeneous microstructures, consisting of soft and hard domains (i.e. small and large grains) to accommodate a gradient of plastic deformation through the increased storage of geometrically necessary dislocations, is particularly interesting to promote strength-ductility synergy [8].

As mentioned in the previous section, the improvement in strain rate sensitivity was observed in several HPT-induced hybrid alloys with increasing numbers of HPT turns. A recent report [195] offered a visual representation of the *m* evolution with increasing numbers of HPT turns from 20 to 60 on the Al–Cu hybrid system (Figure 12) in terms of grain sizes, in comparison with the available data for numerous UFG Al and UFG Cu samples

processed by different SPD techniques (see Figure 15). For a simple visualisation, the general trends are provided by the encircling ovals for the UFG Al and Cu and for the hybrid Al-Cu system. It is apparent that there is a consistent trend of enhanced strain rate sensitivity with grain refinement through SPD processing in both the UFG Al and UFG Cu, except for a few outliers. By contrast, the Al-Cu hybrid system showed excellent improvement in the strain rate sensitivity with a significant grain refinement capability with increasing HPT turns, which is denoted by a red arrow. Considering the high hardness of the Al-Cu hybrid shown in Figure 10(a), the excellent mechanical responses of both strength and strain rate sensitivity lead to the conclusion that the mechanical bonding during grain refinement by HPT is a promising strategy for fabricating hybrid metal systems with exceptional physical and mechanical properties.

A recent work [53] analysed the strain hardening capability of the HPT hybrids for the first time in

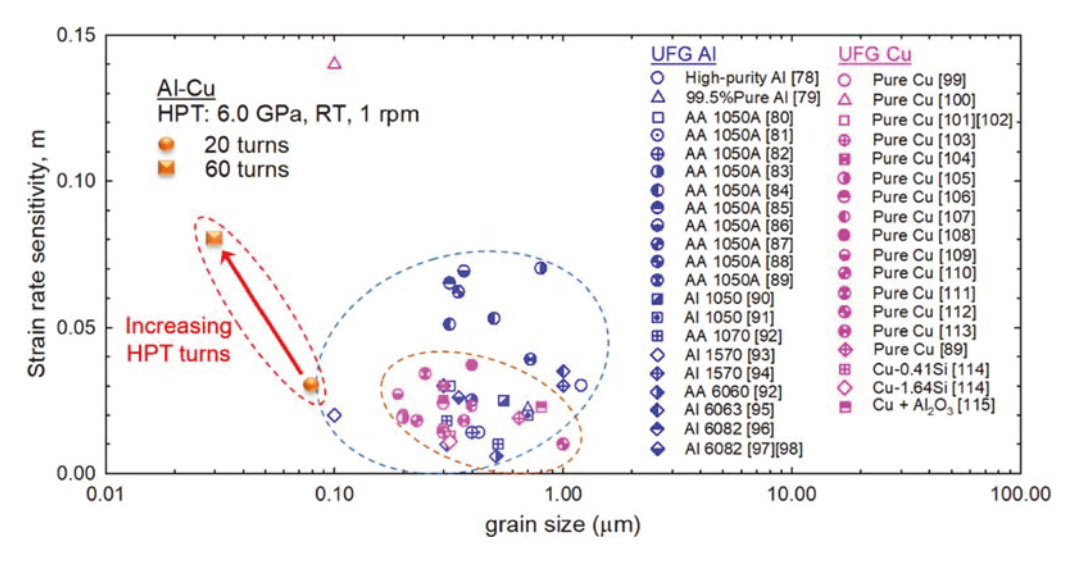


Figure 15. Variation of the strain rate sensitivity with grain size for various UFG Al and UFG Cu processed through different SPD processing procedures and for the HPT-synthesised Al-Cu hybrid system. The encircling ovals provide a visual representation of the trends for Al, for Cu, and for the Al-Cu system [43]. Reproduced with permission from [195].

the Zn-Mg system by utilising the HV measurements recorded along the cross-section of the disk from 1 to 30 turns. The study revealed that Zn-Mg HPT hybrids follow a three-regime behaviour during deformation, which can be observed in the double-natural logarithm plot of the HV values against $\epsilon_{\rm eq}$ shown in Figure 16. The degree of strain hardening associated with each of these regimes was estimated by the value of its slope, which defines the hardenability exponent (η) [196]. Tracking the evolution of the η gives an opportunity to investigate the potential for work hardening, as well as the susceptibility to hardness saturation, which may develop at high strains during SPD processing.

Regime I, up to $\varepsilon_{eq} \sim 30$, indicated a limited strain hardening in the early stage of HPT, with a hardenability exponent of $\eta = 0.017$, which is attributed to moderate grain refinement. Regime II, up to $\varepsilon_{eq} \sim 400$, showed an exceptional strain hardening, with η

= 0.535, which is about one order of magnitude larger than most reported values from conventional HPT processing. For example, commercial alloys processed by HPT, including Ti-6Al-4V [196], ZK60 [197] and AZ31 [198], exhibited values of $\eta = 0.031$, 0.07 and 0.08, respectively. The strain hardening observed in the Zn-Mg HPT hybrids during Regime II was mainly associated with the formation of hard Mg₂Zn₁₁ and MgZn₂ intermetallic compounds and their increased volume fraction at increasing accumulated plastic strain [53]. Regime III, up to $\varepsilon_{eq} \sim 660$, exhibited strain softening, as denoted by the negative η value, which may be related to the saturation of the grain size refinement after severe straining. However, the UFG microstructure developed at the edge after 30 turns exhibited a large volume fraction of high-angle boundaries, which can activate grain boundary sliding at RT [199], and may be responsible for the high m value reported in Figure 14(c). Thus, the transition between

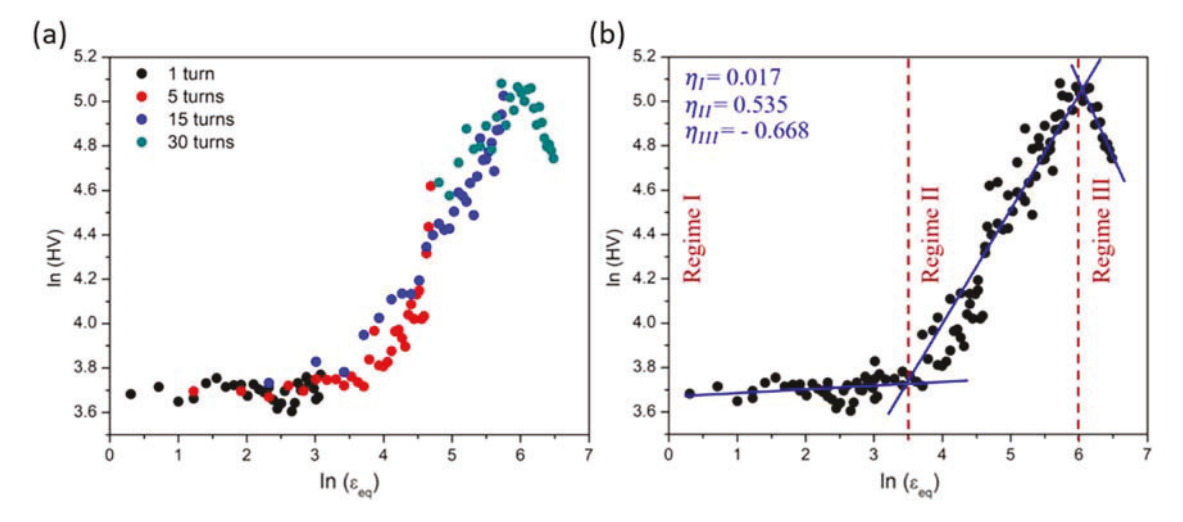


Figure 16. Double-natural logarithm plots of Vickers microhardness (HV) against equivalent strain (ε_{eq}) for the Zn–3Mg HPT hybrid (a) after 1, 5, 15 and 30 turns, and (b) determination of the hardenability exponent (η) in regimes I, II and III, delimited by dash lines. Solid lines indicate the linear regressions. Reproduced with permission from [53].

Regime II and III demonstrated a clear tradeoff in the hardness-plasticity relationship of HPT hybrids.

The observed three-regime strain hardening behaviour was suggested to be due to the activation of multiple strengthening mechanisms, including grain refinement, in-situ precipitation, and back-stress strengthening associated with geometrically necessary dislocations [53]. Although there was no direct measurement of the elongation-to-failure in the latter study, the proven enhancement in both strain hardening and strain rate sensitivity suggested that Zn-Mg hybrids synthesised by HPT + PDA might exhibit an excellent strength-ductility combination owed to their unique heterostructure.

The concept of heterogeneous materials was recently introduced by Wu and Zhu [200] as 'a new class of materials with unprecedented mechanical properties', which exhibit a combination of strength and ductility that are not achievable by their homogenous counterparts. Heterogeneous materials are characterised by multiscale domains (i.e. grains, secondary phase particles) with significant strength differences, such that they will experience different strains during deformation. This will create large strain gradients at the domain interfaces of the heterostructured material, which will produce significant back-stress to increase strength, as well as work hardening for high ductility. Heterogeneous materials are not inherent to a specific deformation process or microstructure. In fact, they have been obtained from a wide variety of structural designs, including bimodal, gradient, lamellar and harmonic microstructures [8]. As shown in the Zn-Mg hybrids above, HPT seems particularly interesting to produce such heterostructured materials, as the process itself subjects the sample to a non-homogeneous plastic strain, which increases with increasing distance from the centre. This resulted in heterogeneous microstructures with different domain sizes, and consequently, a gradienttype hardness distribution across the sample diameter (see Figure 10(e)). Further PDA treatment led to a bimodal grain size distribution with a GS_{ave} of ~ 100-200 nm and $\sim 600-900 \text{ nm}$, acting as hard and soft domains, respectively, and playing complementary roles during plastic deformation [53]. This heterogeneous microstructure obtained after HPT+ PDA resulted in a simultaneous increase of H and m values, which may indicate an enhanced strengthductility combination.

Several other works have evidenced the potential of HPT to achieve strength-ductility synergy after a short annealing treatment in a wide range of materials. For instance, a V-Cr-Mn-Fe-Co-Ni high-entropy alloy (HEA) subjected to HPT for 5 turns and subsequently annealed at 700°C for 10 min resulted in a UTS of 1.54 GPa and an $\varepsilon_f \sim 11\%$ [201]. Such outstanding mechanical properties were related to the contribution

of an intensive dislocation density, ultrafine-grained matrix, and grain boundary precipitation suppressing grain growth. Another work demonstrated the feasibility of HPT to produce an exceptional combination of strength and ductility in a Co-Cr-Fe-Mn-Ni HEA through powder consolidation via HPT for 4 turns followed by annealing at 800°C for 1 h, exhibiting a YS of 754 MPa and an ε_f of 58% [202]. These superlative mechanical properties were attributed to extremely high densification and ultrafine-grained microstructure combined with the minimisation of contamination and undesirable phases. Moreover, this recent work [202] provided a breakthrough in achieving synergy of strength and ductility in the field of powder metallurgy by leveraging the potential of the HPT technique and HEA design concept.

Other studies have also shown good combinations of strength and ductility without any annealing treatment post-HPT. For example, a C nanotube (CNT)reinforced Cu-matrix composite synthesised by a combination of flake powder metallurgy and HPT for 6 turns resulted in a UTS of 474 MPa and an ε_f ~ 11% [203]. This mechanical response was attributed to the formation of a trimodal-grained microstructure with a high density of twin and low angle grain boundaries, together with an adequate interfacial bonding between CNT and Cu. In another work, a Zr-Cu-Al-Ni-Ti bulk metallic glass exhibited simultaneous enhancements of UTS and ϵ_f from 1723 MPa and 0.06% in the as-cast specimen to 2023 MPa and 0.45% after HPT for 30 turns [204]. This synergetic effect was reported to be due to a concurrent increase in free volume (which enhanced the ductility) and nanocrystal precipitation (which increased the strength) during HPT processing, and it was proposed that this strategy may be applicable overall for amorphous-crystalline composites. The strength-ductility synergy from additional HPT-processed materials has also been reported elsewhere [175,205-212].

The application of HPT was proposed as a viable technique to synthesise multiscale architectured materials with composition and grain size gradients, and their mechanical properties were significantly enhanced as compared with those of their homogenous counterparts [213]. Different strategies to design heterostructured materials based on mechanically driven structural and compositional patterning by means of SPD were recently reviewed by Estrin et al. [214]. Similarly, the potential for SPD processes, including HPT, ECAP, ARB, multidirectional forging, and twist extrusion, to engineer materials with multiscale structures was published by Beygelzimer et al. [215] in a chapter of the book 'Architectured Materials in Nature and Engineering'. The two latter works [214,215], together with the studies referenced in the previous two paragraphs, indicated that HPT allows for the manufacturing of hybrid materials with



unprecedented mechanical properties through the combined action of large shear and hydrostatic pressures. This is possible thanks to the different contributions which are characteristic to SPD, such as (1) a significant grain refinement, (2) structural selforganisation of multiphase materials, and (3) unusually fast mass transfer, which can lead to the formation of additional phases [214].

Future potential applications of HPTprocessed components

As stated in the introduction, modern-day severe plastic deformation (SPD) started around 1990. It was a precursor to the boom of nanotechnology that society is feeling the strong impact of today. In 2008, the estimated economic impact of nanotechnology on global markets exceeded 700 billion US dollars [5]. Among the nanomaterials (which were one of the earliest commercial components of nanotechnology) that emerged were bulk nanostructured metals produced by SPD for such applications as pre-forms for forgings, targets for sputtering of precious metals, and sheet for superplastic forming. Since then, HPT-processed metallic hybrids have emerged, and they are demonstrating a significant potential to be considered for commercial applications in a wide variety of industries, including the biomedical, sports, and recreation, electronic, and aerospace industries.

The review by Zhilyaev and Langdon [6] highlighted that SPD materials are especially attractive in fields requiring high specific strengths under extreme conditions and environments, ranging from the use of titanium in the aerospace/defense sector to the use of specialised steels in arctic environments. For the utilisation of HPT-processed parts, it is essential to identify specific areas where HPT offers exceptional advantages by comparison with more conventional processing. Based on the great number of available reports, including experimental results from HPTprocessed materials with properties of interest for specific industries, their potential application in the following major sectors will be presented in the next paragraphs: biomedical implants, microelectronics, magnetic materials, and hydrogen storage materials.

HPT-processed metallic hybrids have shown significant potential in the biomedical industry. For orthopaedic implant applications, the development of materials with favourable surface and bulk properties able to modulate their interactions with the host tissue are fundamental to ensure their success. A recent review on absorbable Zn-based alloys [216], as well as previous works [217,218,227,219-226], have shown the capability of multiple SPD processes to enhance the mechanical properties of pure Zn while maintaining its exceptional degradation behaviour in order to fulfil the requirements of biomedical

applications. Electrochemical testing in simulated body fluid of HPT-processed Zn-Mg hybrids showed that the degree of plastic deformation had an impact on the corrosion resistance of the Zn-Mg hybrids [52]. Both the corrosion mechanism and the electrochemical kinetics were influenced by the number of HPT turns. The current density increased considerably from 1 to 15 turns, as a result of the reactive nature of Mg₂Zn₁₁ and MgZn₂ intermetallics formed during HPT acting as micro-galvanic cells, and then decreased consistently after 30 turns due to higher microstructural uniformity [52]. Zhang et al. [228] reported that a solution treatment prior to HPT processing helped to achieve a more uniform distribution of second phases in a biomedical Mg-Zn-Ca alloy, resulting in higher corrosion resistance in simulated body fluid than the HPT-processed cast alloy. Moreover, the corrosion resistance improved gradually with increasing number of turns, and the alloy exhibited uniform corrosion upon grain size saturation at 130-150 nm after 5 turns [229]. These works demonstrate that absorbable biomedical implants (i.e. Znbased and Mg-based), which are those designed to be dissolved naturally upon tissue healing and regeneration, can benefit from HPT processing to improve their corrosion resistance and mechanical properties simultaneously. Similarly, permanent biomedical implants (i.e. Ti-based and Co-based), which are typically preferred to withstand larger body loads (i.e. hip stem and knee prosthesis), have also demonstrated improved strength and hardness [230,231], as well as enhanced cell adhesion [232] upon HPT processing. For example, the nature and mechanisms of the cellsubstrate interaction were assessed for HPT-processed Ti [233,234], and it was shown that the degree of preosteoblast attachment and growth rate were both markedly increased on the substrates after HPT processing. The simultaneous improvement in cell activity was attributed to the nanostructured feature of the substrates, thus, demonstrating the advantages of processing titanium by HPT for biomedical applications by comparison with conventional and coated Ti implants. In addition, recent investigations on biocompatible Ti-Nb alloys processed by HPT have shown a promising combination of strength, ductility, and Youngs modulus close to that of human bone, confirming their potential for future orthopaedic devices [235,236].

Another potential application where HPT-processed hybrids may find their path into the market is in the microelectronics industry. Micro-electro-mechanical systems (MEMS) are characterised for requiring exceptional mechanical and functional properties in components with very small sizes (i.e. microscale to nanoscale). The development of Al-based and Cubased MEMS by incorporating low dimensional carbon allotropes, such as graphene, has drawn special attention for applications in integrated circuits, chips, and micro/nano-wires [237]. For example, Huang et al. [94] reported that graphene-reinforced Al hybrids synthesised by HPT exhibited a simultaneous enhancement of hardness, tensile strength, and electrical conductivity, as compared to HPT-processed commercial Al. Similarly, Khobragade et al. [95] demonstrated a significant dual increase in hardness and electrical conductivity in Cu-graphene nanocomposites produced by HPT, as compared to pure Cu processed under similar conditions. The main reason why the previous two examples improved their electrical conductivity by limiting electron scattering upon HPT processing is the combination of extensive grain refinement with the formation of nanosized second phases [238]. Several other investigations [19,187,203,239] have also confirmed that HPT is a promising pathway to obtain materials with a good combination of tensile properties and electrical conductivity. Moreover, conventional HPT samples (i.e. 1 mm thickness and 10 mm diameter) would be feasible to produce small-scale components of similar sizes used in MEMs applications. Thereby, their manufacturing would be relatively simple and may be undertaken with a minimum number of separate processing operations.

HPT-processed hybrids are also of interest in the field of magnetic materials due to the dramatic change in their hysteresis properties. Tailored magnetic properties, including diamagnetism, paramagnetism, and ferromagnetism, can be achieved through HPT by extensively refining not only the grain size, but also the size and distribution of second phase particles. Ferromagnetic particles can be finely dispersed within the matrix of non-magnetic materials, leading to magnetoresistance, which is characterised by an isotropic behaviour, unlike conventional ferromagnets [240]. HPT has been extensively explored as a mechanism to disperse such particles, typically with little solubility in the matrix, as they are not intended to form a solid solution. Thus, several investigations [20,21,241] in HPT-processed immiscible systems, such as the Cu-Co and Cu-Fe systems, have reported an exceptional magnetoresistance at RT. These studies also highlighted the capability of HPT for controlling other magnetic properties, like magnetisation and coercivity. Deformation-induced phase transformations and metastable phase formation during HPT have also been related to an improvement of magnetic properties in Nd/Pr-Fe-B ternary alloys [242-245], which gave rise to the most widely used permanent magnets since they were first introduced in the 1980s. Moreover, HPT-processed α-Fe/Nd-Fe-B nanocomposite magnets exhibited a simultaneous enhancement of both magnetisation and coercivity, which are generally mutually exclusive properties, due to the high fraction of soft-magnetic phase and the enhancement in

domain wall pinning strength [246]. HPT also offers the opportunity to discover new magnetic materials. For example, Cepeda-Jiménez et al. [247] showed that pure Hf, a classical paramagnet, can become ferromagnetic after HPT processing due to the development of a new monoclinic phase that exhibits spontaneous magnetisation. All these works evidence that there exists is a great variety of materials that can benefit from HPT processing to produce heterogeneous microstructures with different domain sizes that lead to enhanced magnetic properties.

Hydrogen has emerged as a clean energy carrier in the last few years, and consequently, the investigation of alternative hydrogen storage systems beyond the conventional pressurised tanks has recently become a hot topic. Hydrogen can also be stored in reversible, solid-state, light metal hydrides (such as Mg, MgNi2, LaNi5, or TiFe), but they typically exhibit slow kinetics in the charging/discharging processes and high hydrogen desorption temperatures. However, the kinetics can be significantly improved by reducing the GS_{ave} and/or introducing large densities of lattice defects, which enhance diffusion and can act as pathways for hydrogen transport [238]. These effects have been demonstrated in numerous HPT-processed hybrids, mainly Mg-based and Ti-based, and their major findings were reviewed by Edalati et al. [248]. Both Mg and Ti are highly reactive and can store hydrogen in the form of MgH2 and TiH2, respectively. Moreover, the Mg-Ti binary system is immiscible even in liquid form; however, processing by HPT enables the formation of four different metastable Mg-Ti phases. After hydrogenation, these Mg-Ti phases decomposed during heating before they can form Mg-Ti hydrides, and thus, only MgH₂ and TiH₂ contributed to hydrogen storage, but only to a limited extent due to their thermodynamic stability [249]. One approach to overcome this issue resulted in the use of HPT to synthesise Mg_2X compounds (X = 21 different elements) to investigate the formation of metastable phases/ intermetallics with hydrogen storage potential [250]. The study concluded that the hydrogen desorption temperature decreased with the addition of elements, which resulted in an increased hydrogen storage capacity, and the desorption temperature can be correlated with the theoretical hydrogen binding energies obtained from first-principle calculations. Similar to Mg and Ti, Zr is another potential candidate for hydrogen storage in the form of ZrH₂. The HPT processing of the Mg-Zr system, which is immiscible in both solid and liquid states like the Mg-Ti system, enabled the formation of several Mg-Zr metastable phases. These phases did not decompose until 500 ° C and demonstrated reversible hydrogen storage capability at RT [251]. HPT-processed Mg-based ternary compounds have also been explored, like the Mg-Ni-Sn system, which exhibited high phase stability up to 167°C and reversible hydrogenation properties at RT [252]. These works highlight the potential of HPT as a suitable technique for the production of hydrogen storage materials, as it has improved not only their hydrogenation kinetics, but also the hydrogenation activity by enhancing the air resistivity and synthesising new nanostructured hydrogen storage phases.

The evident potential of HPT hybrids to produce materials with an unprecedented set of properties for a wide range of high-demanding applications is certainly exciting. Despite the small sample size and lack of continuous processing characteristic of the conventional HPT procedure, current and future researchers in the field should not be discouraged from pursuing the industrialisation of their scientific breakthroughs. To facilitate this transition from laboratory to market, novel severe straining processes inspired by conventional HPT principles, namely high-pressure sliding, high-pressure compressive sliding, and continuous high-pressure torsion, are currently under development.

Summary and concluding remarks

The investigation of metal hybrids processed by HPT is still at an early stage, and it is anticipated to skyrocket over the next few years due to the inherent capability of HPT to produce heterostructured materials with mechanical and functional properties of interest for highly demanding applications. Not only is HPT considered one of the most efficient SPD processes in terms of grain refinement, but it also offers versatility for designing new materials, as well as exploring alternative experimental setups and processing parameters. The extensive literature survey presented in this review article highlights the feasibility of adapting the principles of conventional HPT, developed by Bridgman back in 1935, to produce compact samples from mechanical bonding of dissimilar metals through solid-state reactions at RT. This approach has gained popularity in the last decade, as HPT-processed hybrids exhibit UFG microstructures (i.e. within the microscale and/or nanoscale regime), which are heterogeneous across the disk diameter, according to the shear strain distribution during HPT. It is precisely this microstructural heterogeneity, characterised by multiscale domains (i.e. grains, secondary phases, precipitates), that conveys a unique combination of properties not achievable by homogeneous counterparts.

Undoubtedly, HPT has demonstrated a promising potential to synthesise heterostructured metal hybrids with mechanical and functional properties that could outperform those of specific products currently used in a wide range of engineering industrial applications. Nevertheless, due to the relatively young age of this approach, there are still several knowledge gaps to be

filled and challenges that must be addressed before HPT hybrids can attract commercial interest. For example, a deeper understanding of the fundamental aspects governing HPT-induced microstructural transformations, such as in situ phase formations or crystalline-to-amorphous transitions, is required in order to have better control over the resulting hybrid microstructures. Further progress to expand our current knowledge in this area could result from an interdisciplinary collaboration between experimental and computational teams of experts within the field of materials science. The standardisation of mechanical testing for HPT-processed samples is another relevant issue to consider. To date, researchers have evaluated mechanical properties, like tensile or fatigue strength, using different testing geometries obtained from different locations within the HPT sample. This precludes the comparison of mechanical properties between different studies, given the inherent inhomogeneity of the HPT procedure. Therefore, current testing standard methods should be revisited in order to provide a consistent framework to enable the evaluation and meaningful comparison of the mechanical properties in HPT-processed samples. Another aspect hampering the implementation of HPT in industrial applications is the limited product size of conventional samples (i.e. 10 mm diameter, 1 mm thickness), which is associated with the massive pressures needed to produce such a level of plastic deformation. However, significant advancements in upscaling the HPT procedure in recent years have led to samples up to 60 mm diameter and 12 mm thickness, which could make them attractive candidates for specific commercial applications. Lastly, it is worth acknowledging the recent surge of alternative HPT-inspired processes for the production of continuous production of sheet metal, including HPS, HPCS, and CHPT, which have an enormous potential for industrial feasibility.

Acknowledgements

The authors acknowledge the graphical assistance provided by Dr. Natalia Pajares-Chamorro (Michigan State University) and useful discussions with Dr. Hakan Yilmazer (Yildiz Technical University, Istanbul, Turkey) and Dr. Hendra Hermawan (Laval University, Montreal, Canada).

Disclosure statement

No potential conflict of interest was reported by the author(s).

Funding

This work was supported by the National Science Foundation (US) - Division of Materials Research under [Grant Number DMR-1607942] through the Metals and Metallic



Nanostructures (MMN) program (DHE & CJB) and under [Grant Number DMR-1810343 (MK)].

ORCID

David Hernández-Escobar http://orcid.org/0000-0001-6133-5259

Megumi Kawasaki http://orcid.org/0000-0003-0028-3007 Carl J. Boehlert http://orcid.org/0000-0001-8051-1051

References

- [1] Valiev RZ, Estrin Y, Horita Z, et al. Producing bulk ultrafine-grained materials by severe plastic deformation: Ten years later. JOM. 2016;68:1216-1226. doi:10.1007/s11837-016-1820-6
- [2] Valiev RZ, Estrin Y, Horita Z, et al. Fundamentals of Superior properties in bulk NanoSPD materials. Mater Res Lett. 2015;3831:1-21. doi:10.1080/ 21663831.2015.1060543
- [3] Valiev RZ, Islamgaliev RK, Alexandrov IV. Bulk nanostructured materials from severe plastic deformation. Prog Mater Sci. 2000;45:103-189. doi:10. 1016/S0079-6425(99)00007-9
- [4] Wang JT. Historic retrospection and present status of severe plastic deformation in China, in: mater. Sci Forum. 2006: 363-370. doi:10.4028/www.scientific. net/msf.503-504.363
- [5] Lowe TC, Zhu YT. Commercialization of nanostructured metals produced by severe plastic deformation processing. Adv Eng Mater. 2003;5:373-378. doi:10. 1002/adem.200310076
- [6] Zhilyaev AP, Langdon TG. Using high-pressure torsion for metal processing: Fundamentals and applications. Prog Mater Sci. 2008;53:893-979. doi:10. 1016/j.pmatsci.2008.03.002
- [7] Valiev R. Nanostructuring of metals by severe plastic deformation for advanced properties. Nat Mater. 2004;3:511-516. doi:10.1038/nmat1180
- [8] Ma E, Zhu T. Towards strength-ductility synergy through the design of heterogeneous nanostructures in metals. Mater Today. 2017;20:323-331. doi:10. 1016/J.MATTOD.2017.02.003
- [9] Wang Y, Chen M, Zhou F, et al. High tensile ductility in a nanostructured metal. Nature. 2002;419:912-915. doi:10.1038/nature01133
- [10] Wang L, Shi Y, Zhang Y, et al. High tensile ductility and strength in a gradient structured Zr. Mater Lett. 2018;228:500-503. doi:10.1016/j.matlet.2018.06.084
- [11] Youssef KM, Scattergood RO, Murty KL, et al. Ultrahigh strength and high ductility of bulk nanocrystalline copper. Appl Phys Lett. 2005;87:091904. doi:10.1063/1.2034122
- [12] Vinogradov A, Orlov D, Estrin Y. Improvement of fatigue strength of a Mg-Zn-Zr alloy by integrated extrusion and equal-channel angular pressing. Scr Mater. 2012;67:209–212. doi:10.1016/j.scriptamat. 2012.04.021
- [13] Ueno H, Kakihata K, Kaneko Y, et al. Enhanced fatigue properties of nanostructured austenitic SUS 316L stainless steel. Acta Mater. 2011;59:7060-7069. doi:10.1016/j.actamat.2011.07.061
- [14] Figueiredo RB, Eduardo ER, Zhao X, et al. Improving the fatigue behavior of dental implants through processing commercial purity titanium by equal-channel

- angular pressing. Mater Sci Eng A. 2014;619:312-318. doi:10.1016/j.msea.2014.09.099
- [15] Horita Z, Furukawa M, Nemoto M, et al. Superplastic forming at high strain rates after severe plastic deformation. Acta Mater. 2000;48:3633-3640. doi:10. 1016/S1359-6454(00)00182-8
- [16] Kawasaki M, Langdon TG. Developing superplasticity and a deformation mechanism map for the Zn-Al eutectoid alloy processed by high-pressure torsion. Mater Sci Eng A. 2011;528:6140-6145. doi:10. 1016/j.msea.2011.04.053
- [17] Shangina DV, Gubicza J, Dodony E, et al. Improvement of strength and conductivity in Cualloys with the application of high pressure torsion and subsequent heat-treatments. J Mater Sci. 2014: 6674-6681. doi:10.1007/s10853-014-8339-4
- [18] Edalati K, Imamura K, Kiss T, et al. Equal-Channel angular pressing and high-pressure torsion of pure copper: evolution of electrical conductivity and hardness with strain. Mater Trans. 2012;53:123-127. doi:10.2320/matertrans.MD201109
- [19] Cubero-Sesin JM, In H, Arita M, et al. High-pressure torsion for fabrication of high-strength and highelectrical conductivity Al micro-wires. J Mater S. 2014: 6550-6557. doi:10.1007/s10853-014-8240-1
- [20] Suehiro K, Nishimura S, Horita Z, et al. Highpressure torsion for production of magnetoresistance in Cu-Co alloy. J Mater Sci. 2008;43:7349-7353. doi:10.1007/s10853-008-2813-9
- [21] Nishihata S, Suehiro K, Arita M, et al. High-Pressure torsion for Giant magnetoresistance and better magnetic properties. Adv Eng Mater. 2010;12:793-797. doi:10.1002/adem.201000033
- [22] Krystian M, Zehetbauer MJ, Kropik H, et al. Hydrogen storage properties of bulk nanostructured ZK60 Mg alloy processed by equal channel angular pressing. J Alloys Compd. 2011: S449-S455. doi:10. 1016/j.jallcom.2011.01.029
- [23] Huot J, Skryabina NY, Fruchart D. Application of severe plastic deformation techniques to magnesium for enhanced hydrogen sorption properties. Metals (Basel). 2012;2:329-343. doi:10.3390/met2030329
- [24] Nishizaki T, Lee S, Horita Z, et al. Superconducting properties in bulk nanostructured niobium prepared by high-pressure torsion. Phys Cond Supercond Appl. 2013;493:132–135. doi:10.1016/j.physc.2013. 03.046
- [25] Edalati K, Daio T, Lee S, et al. High strength and superconductivity in nanostructured niobium-titanium alloy by high-pressure torsion and annealing: significance of elemental decomposition and supersaturation. Acta Mater. 2014;80:149-158. doi:10. 1016/j.actamat.2014.07.065
- [26] Bridgman PW. On torsion combined with compression. J Appl Phys. 1943;14:273-283. doi:10. 1063/1.1714987
- [27] Bridgman PW. Effects of high shearing stress combined with high hydrostatic pressure. Phys Rev. 1935;48:825-847. [cited 2018 Nov 21]. https:// journals.aps.org/pr/pdf/10.1103/PhysRev.48.825.
- [28] Bridgman PW. Studies in large plastic flow and fracture - With special emphasis on the effects of hydrostatic pressure. Cambridge, MA: Harvard University Press; 1964. doi:10.4159/harvard.9780674731349.
- [29] Segal VM, Reznikov VI, Drobyshevskiy A, et al. Plastic working of metals by simple shear. Russ Metall. 1981;1:99-105. [cited 2021 Jan 23]. https://



- www.scirp.org/(S(vtj3fa45qm1ean45vvffcz55))/reference/ReferencesPapers.aspx?ReferenceID=2026248.
- [30] Segal VM. Materials processing by simple shear. Mater Sci Eng A. 1995;197:157-164. doi:10.1016/ 0921-5093(95)09705-8
- [31] Saito Y, Utsunomiya H, Tsuji N, et al. Novel ultrahigh straining process for bulk materials—development of the accumulative roll-bonding (ARB) process. Acta Mater. 1999;47:579-583. doi:10.1016/ \$1359-6454(98)00365-6
- [32] Saito Y, Tsuji N, Utsunomiya H, et al. Ultra-fine grained bulk aluminum produced by accumulative roll-bonding (ARB) process. Scr Mater. 1998;39:1221–1227. doi:10. 1016/S1359-6462(98)00302-9
- [33] Hohenwarter A, Bachmaier A, Gludovatz B, et al. Technical parameters affecting grain refinement by high pressure torsion. Int J Mater Res. 2009: 1653-1661. doi:10.3139/146.110224
- [34] Han J-K, Jang J, Langdon TG, et al. Bulk-state reactions and improving the mechanical properties of metals through high-pressure torsion. Mater Trans. 2019;60:1131-1138. doi:https://doi.org/10.2320/ matertrans.MF201908
- [35] Valiev RZ, Ivanisenko YV, Rauch EF, et al. Structure and deformaton behaviour of Armco iron subjected to severe plastic deformation. Acta Mater. 1996;44:4705-4712. doi:10.1016/S1359-6454 (96)00156-5
- [36] Polakowski N, Ripling E. Strength and structure of engineering materials. Englewood Cliffs: Prentice-
- [37] Kapoor R. Severe plastic deformation of materials. Mater Under Extrem Cond. 2017: 717-754. doi:10. 1016/B978-0-12-801300-7.00020-6
- [38] Oh-ishi K, Edalati K, Kim HS, et al. High-pressure torsion for enhanced atomic diffusion and promoting solid-state reactions in the aluminum-copper system. Acta Mater. 2013;61:3482-3489. doi:10. 1016/J.ACTAMAT.2013.02.042
- [39] Han J-K, Han DK, Liang GY, et al. Direct bonding of aluminum-copper metals through high-pressure torsion processing. Adv Eng Mater. 2018;20:1800642. doi:10.1002/adem.201800642
- [40] Danilenko VN, Sergeev SN, Baimova JA, et al. An approach for fabrication of Al-Cu composite by high pressure torsion. Mater Lett. 2019;236:51-55. doi:10.1016/j.matlet.2018.09.158
- [41] Kawasaki M, Ahn B, Lee H-J, et al. Using highpressure torsion to process an aluminum-magnesium nanocomposite through diffusion bonding. Acta Mater. 2015;59:1974-1985. doi:10.1016/j. actamat.2010.11.063
- [42] Han JK, Lee HJ, il Jang J, et al. Micro-mechanical and tribological properties of aluminum-magnesium nanocomposites processed by high-pressure torsion. Mater Sci Eng A. 2017;684:318-327. doi:10.1016/j. msea.2016.12.067
- [43] Kawasaki M, Jung SH, Park JM, et al. Mechanical Bonding of Aluminum Hybrid Alloy Systems through high-pressure torsion. Adv Eng Mater. 2020;22:1900483. doi:10.1002/adem.201900483.
- [44] Kawasaki M, Jang J. Micro-Mechanical response of an Al-Mg hybrid system synthesized by highpressure torsion. Materials (Basel). 2017;10:596. doi:10.3390/ma10060596
- [45] Ahn B, Lee HJ, Choi IC, et al. Micro-Mechanical behavior of an exceptionally strong metal matrix

- nanocomposite processed by high-pressure torsion. Adv Eng Mater. 2016;18:1001-1008. doi:10.1002/ adem.201500520
- [46] Kawasaki M, Han J-K, Lee D-H, et al. Fabrication of nanocomposites through diffusion bonding under high-pressure torsion. J Mater Res. 2018: 1-11. doi:10.1557/jmr.2018.205
- Han J-K, Park J-M, Ruan W, et al. Size effect on microstructural evolution and micromechanical responses of mechanically bonded aluminum and magnesium by high-pressure torsion. Adv Eng Mater. 2019;1900971; doi:10.1002/adem.201900971
- [48] Ibrahim N, Peterlechner M, Emeis F, et al. Mechanical alloying via high-pressure torsion of the immiscible Cu50Ta50 system. Mater Sci Eng A. 2017;685:19-30. doi:https://doi.org/10.1016/j.msea.2016.12.106
- [49] Qi Y, Kosinova A, Kilmametov AR, et al. Plastic flow and microstructural instabilities during high-pressure torsion of Cu/ZnO composites. Mater Charact. 2018;145:389–401. doi:10.1016/j.matchar.2018.09.001
- [50] Rogachev SO, Sundeev RV, Khatkevich VM. Evolution of the structure and strength of steel/ vanadium alloy/steel hybrid material during severe plastic deformation. Mater Lett. 2016;173:123-126. doi:10.1016/j.matlet.2016.03.044
- [51] Rogachev SO, Nikulin SA, Rozhnov AB, et al. Multilayer "steel/vanadium alloy/steel" hybrid material obtained by high-pressure torsion at differtemperatures. Metall Mater Trans A. 2017;48:6091-6101. doi:10.1007/s11661-017-4342-0
- [52] Hernández-Escobar D, Rahman ZU, Yilmazer H, et al. Microstructural evolution and intermetallic formation in Zn-Mg hybrids processed by high-pressure torsion. Philos Mag. 2019;99:557-584. doi:10.1080/ 14786435.2018.1546962
- [53] Hernández-Escobar D, Marcus J, Han J-K, et al. Effect of post-deformation annealing on the microstructure and micro-mechanical behavior of Zn-Mg hybrids processed by high-pressure torsion. Mater Sci Eng A. 2020;771:138578. doi:https://doi. org/10.1016/j.msea.2019.138578
- [54] Hernández-Escobar D, Unocic RR, Kawasaki M, et al. High-pressure torsion processing of Zn-3Mg alloy and its hybrid counterpart: a comparative study. J. Alloys Compd. 2020;831:154891. doi:10. 1016/j.jallcom.2020.154891
- [55] Rogachev SO, Nikulin SA, Khatkevich VM, et al. Structure formation and hardening of the hybrid material based on Vanadium and zirconium alloys during high-pressure torsion. Russ. Metall. 2018;2018:372-376. doi:10.1134/S0036029518040110
- [56] Li L, Nagai K, Yin F. Progress in cold roll bonding of metals. Sci Technol Adv Mater. 2008;9:023001. doi:10.1088/1468-6996/9/2/023001
- [57] Min G, Lee JM, Kang SB, et al. Evolution of microstructure for multilayered Al/Ni composites by accumulative roll bonding process. Mater Lett. 2006;60:3255–3259. doi:10.1016/j.matlet.2006.03.001
- [58] Chen MC, Hsieh HC, Wu W. The evolution of microstructures and mechanical properties during accumulative roll bonding of Al/Mg composite. J. Alloys Compd. 2006;416:169-172. doi:10.1016/j. jallcom.2005.09.017
- [59] Du Y, Fan G, Yu T, et al. Laminated Ti-Al composites: processing, structure and strength. Mater Sci Eng A. 2016;673:572-580. doi:10.1016/j.msea.2016. 07.108



- [60] Ebrahimi SHS, Dehghani K, Aghazadeh J, et al. Investigation on microstructure and mechanical properties of Al/Al-Zn-Mg-Cu laminated composite fabricated by accumulative roll bonding (ARB) process. Mater Sci Eng A. 2018;718:311-320. doi:10. 1016/j.msea.2018.01.130
- [61] Zeng LF, Gao R, Fang QF, et al. High strength and thermal stability of bulk Cu/Ta nanolamellar multilayers fabricated by cross accumulative roll bonding. Acta Mater. 2016;110:341–351. doi:10.1016/j. actamat.2016.03.034
- [62] Beausir B, Scharnweber J, Jaschinski J, et al. Plastic anisotropy of ultrafine grained aluminium alloys produced by accumulative roll bonding. Mater Sci Eng A. 2010;527:3271–3278. doi:10.1016/j.msea. 2010.02.006
- [63] Azushima A, Kopp R, Korhonen A, et al. Severe plastic deformation (SPD) processes for metals. CIRP Ann - Manuf Technol. 2008;57:716-735. doi:10. 1016/j.cirp.2008.09.005
- [64] Sun YF, Fujii H, Tsuji N, et al. Fabrication of ZrAlNiCu bulk metallic glass composites containing pure copper particles by high-pressure torsion. J Alloys Compd. 2010;492:149-152. doi:10.1016/j. jallcom.2009.11.135
- [65] Sun YF, Fujii H, Nakamura T, et al. Critical strain for mechanical alloying of Cu-Ag, Cu-Ni and Cu-Zr by high-pressure torsion. Scr Mater. 2011;65:489-492. doi:10.1016/j.scriptamat.2011.06.005
- [66] Miyazaki T, Terada D, Miyajima Y, et al. Synthesis of non-equilibrium phases in immiscible metals mechanically mixed by high pressure torsion. J Mater Sci. 2011;46; 4296-4301. doi:10.1007/s10853-010-5240-7
- [67] Bouaziz O, Kim HS, Estrin Y. Architecturing of metal-based composites with concurrent nanostructuring: a new paradigm of materials design. Adv Eng Mater. 2013;15:336-340. doi:10.1002/adem. 201200261
- [68] Ahn B, Zhilyaev AP, Lee H-J, et al. Rapid synthesis of an extra hard metal matrix nanocomposite at ambient temperature. Mater Sci Eng A. 2015;635:109-117. doi:10.1016/j.msea.2015.03.042
- [69] Kawasaki M, Ahn B, Lee H, et al. Using high-pressure torsion to process an aluminum-magnesium nanocomposite through diffusion bonding. J Mater Res. 2016;31:88–99. doi:10.1557/jmr.2015.257
- [70] Kawasaki M, Jung SH, Park J-M, et al. Mechanical bonding of aluminum hybrid alloy systems through torsion. Adv high-pressure Eng 2020;22:1900483. doi:10.1002/adem.201900483
- [71] Okeke U, Yilmazer H, Sato S, et al. Strength enhancement of an aluminum alloy through high pressure torsion. Mater Sci Eng A. 2019;760:195-205. doi:10. 1016/j.msea.2019.05.102
- [72] Todaka Y, Umemoto M, Yamazaki A, et al. Effect of strain path in high-pressure torsion process on hardening in commercial purity titanium. Mater Trans. 2008;49:47-53. doi:10.2320/matertrans.ME200714
- [73] Sabirov I, Pippan R. Formation of a W-25%Cu nanocomposite during high pressure torsion. Scr Mater. 2005;52:1293-1298. doi:10.1016/J.SCRIPTAMAT. 2005.02.017
- [74] Zhilyaev AP, Nurislamova GV, Kim BK, et al. Experimental parameters influencing grain refinement and microstructural evolution during high-

- pressure torsion. Acta Mater. 2003;51:753-765. doi:10.1016/S1359-6454(02)00466-4
- Sakai G, Nakamura K, Horita Z, et al. Developing high-pressure torsion for use with bulk samples. Mater Sci Eng A. 2005;406:268-273. doi:10.1016/j. msea.2005.06.049
- [76] Pippan R, Scheriau S, Hohenwarter A, et al. Advantages and limitations of HPT: a review. Mater Sci Forum. 2008;584-586:16-21. doi:10.4028/ www.scientific.net/MSF.584-586.16
- [77] Hohenwarter A, Pippan R. Sample size and strainrate-sensitivity effects on the homogeneity of highpressure torsion deformed disks. Metall Mater Trans A Phys Metall Mater Sci. 2019;50:601-608. doi:10.1007/s11661-018-4989-1
- [78] Fujioka T, Horita Z. Development of high-pressure sliding process for microstructural refinement of rectangular metallic sheets. Mater Trans. 2009;50:930-933. doi:10.2320/matertrans.MRP2008445
- [79] Takizawa Y, Masuda T, Fujimitsu K, et al. Scaling up of high-pressure sliding (HPS) for grain refinement and superplasticity. Metall Mater Trans A Phys Metall Mater Sci. 2016;47:4669-4681. doi:10.1007/ s11661-016-3623-3
- [80] Toth LS, Vu VQ, Dhinwal SS, et al. The mechanics of high pressure compressive shearing with application to ARMCO® steel. Mater Charact. 2019;154:127-137. doi:10.1016/j.matchar.2019.05.039
- [81] Edalati K, Horita Z. Continuous high-pressure torsion. J Mater Sci. 2010;45:4578-4582. doi:10.1007/ s10853-010-4381-z
- [82] Lee Z, Zhou F, Valiev RZ, et al. Microstructure and microhardness of cryomilled bulk nanocrystalline Al-7.5%Mg alloy consolidated by high pressure torsion. Scr Mater. 2004;51:209-214. doi:10.1016/j. scriptamat.2004.04.016
- [83] Cubero-Sesin JM, Horita Z. Powder consolidation of Al-10wt% Fe alloy by High-Pressure Torsion. Mater Sci Eng A. 2012;558:462-471. doi:10.1016/j.msea.
- [84] Kreuzeder M, Abad MD, Primorac MM, et al. Fabrication and thermo-mechanical behavior of ultra-fine porous copper. J Mater Sci. 2015;50:634-643. doi:10.1007/s10853-014-8622-4
- [85] Leitner A, Maier-Kiener V, Jeong J, et al. Interface dominated mechanical properties of ultra-fine grained and nanoporous Au at elevated temperatures. Acta Mater. 2016;121:104-116. doi:10.1016/j. actamat.2016.08.071
- [86] Wurmshuber M, Frazer D, Bachmaier A, et al. Impact of interfaces on the radiation response and underlying defect recovery mechanisms in nanostructured Cu-Fe-Ag. Mater Des. 2018;160:1148-1157. doi:10.1016/j.matdes.2018.11.007
- Alexandrov IV, Zhu YT, Lowe TC, et al. Microstructures and properties of nanocomposites obtained through SPTS consolidation of powders. Metall Mater Trans A Phys Metall Mater Sci. 1998;29:2253-2260. doi:10.1007/s11661-998-0103-4
- [88] Ashida M, Horita Z, Kita T, et al. Production of Al/ Al₂O₃ nanocomposites through consolidation by high-pressure torsion. Mater Trans. 2012;53:13-16. doi:10.2320/matertrans.MD201128
- [89] Stolyarov VV, Zhu YT, Lowe TC, et al. Processing nanocrystalline Ti and its nanocomposites from micrometer-sized Ti powder using high pressure

- - torsion. Mater Sci Eng A. 2000;282:78-85. doi:10. 1016/S0921-5093(99)00764-9
- [90] Menéndez E, Sort J, Langlais V, et al. Cold compaction of metal-ceramic (ferromagnetic-antiferromagnetic) composites using high pressure torsion. J Alloys Compd. 2007;434-435:505-508. doi:10.1016/ j.jallcom.2006.08.142
- [91] Menéndez E, Salazar-Alvarez G, Zhilyaev AP, et al. Cold consolidation of metal-ceramic nanocomposite powders with large ceramic fractions. Adv Funct 2008;18:3293-3298. doi:10.1002/adfm. Mater. 200800456
- [92] Grosdidier T, Fundenberger JJ, Zou JX, et al. Nanostructured Mg based hydrogen storage bulk materials prepared by high pressure torsion consolidation of arc plasma evaporated ultrafine powders. Int J Hydrogen Energy. 2015;40:16985-16991. doi:10.1016/j.ijhydene.2015.06.159
- [93] Zhao L, Lu H, Gao Z. Microstructure and mechanical properties of Al/graphene composite produced by high-pressure torsion. Adv Eng Mater. 2015;17:976-981. doi:10.1002/adem.201400375
- [94] Huang Y, Bazarnik P, Wan D, et al. The fabrication of graphene-reinforced Al-based nanocomposites using high-pressure torsion. Acta 2019;164:499-511. doi:10.1016/J.ACTAMAT.2018. 10.060
- [95] Khobragade N, Sikdar K, Kumar B, et al. Mechanical and electrical properties of copper-graphene nanocomposite fabricated by high pressure torsion. J Alloys Compd. 2019;776:123-132. doi:10.1016/j. jallcom.2018.10.139
- [96] Korznikova G, Czeppe T, Khalikova G, et al. Microstructure and mechanical properties of Cu-graphene composites produced by two high pressure procedures. Mater 2020;161:110122. doi:10.1016/j.matchar.2020.110122
- [97] Tokunaga T, Kaneko K, Horita Z. Production of aluminum-matrix carbon nanotube composite using high pressure torsion. Mater Sci Eng A. 2008;490:300-304. doi:10.1016/J.MSEA.2008.02.022
- [98] Asgharzadeh H, Joo SH, Kim HS. Consolidation of carbon nanotube reinforced aluminum matrix composites by high-pressure torsion. Metall Mater Trans A Phys Metall Mater Sci. 2014;45:4129-4137. doi:10.1007/s11661-014-2354-6
- [99] Jenei P, Gubicza J, Yoon EY, et al. High temperature thermal stability of pure copper and copper-carbon nanotube composites consolidated by high pressure torsion. Compos Part A Appl Sci Manuf. 2013;51:71-79. doi:10.1016/J.COMPOSITESA.2013. 04.007
- [100] Jenei P, Yoon EY, Gubicza J, et al. Microstructure and hardness of copper-carbon nanotube composites consolidated by high pressure torsion. Mater Sci Eng A. 2011;528:4690-4695. doi:10.1016/J. MSEA.2011.02.066
- [101] Edalati K, Toh S, Ikoma Y, et al. Plastic deformation and allotropic phase transformations in zirconia ceramics during high-pressure torsion. Scr Mater. 2011;65:974–977. doi:10.1016/j.scriptamat.2011.08. 024
- [102] Edalati K, Iwaoka H, Toh S, et al. Application of high-pressure torsion to WC-Co ceramic-based composites for improvement of consolidation, microstructure and hardness. Mater Trans. 2013;54:1540-1548. doi:10.2320/matertrans.MH201318

- [103] Hidalgo-Jimenez J, Wang Q, Edalati K, et al. Phase transformations, vacancy formation and variations of optical and photocatalytic properties in TiO2-ZnO composites by high-pressure torsion. Int J Plast. 2020;124:170–185. doi:10.1016/j.ijplas.2019.08.010
- Edalati K, Uehiro R, Takechi S, et al. Enhanced photocatalytic hydrogen production on GaN-ZnO oxynitride by introduction of strain-induced nitrogen vacancy complexes. Acta Mater. 2020;185:149-156. doi:10.1016/j.actamat.2019.12.007
- [105] Castro MM, Pereira PHR, Isaac A, et al. Development of a magnesium-alumina composite through cold consolidation of machining chips by high-pressure torsion. I Alloys Compd. 2019;780:422-427. doi:10.1016/j.jallcom.2018.11.357
- [106] Zhilyaev AP, Gimazov AA, Raab GI, et al. Using high-pressure torsion for the cold-consolidation of copper chips produced by machining. Mater Sci Eng A. 2008;486:123–126. doi:10.1016/j.msea.2007.
- [107] Abd El Aal MI, Yoo Yoon E, Seop Kim H. Recycling of AlSi8Cu3 alloy chips via high pressure torsion. Mater Sci Eng A. 2013;560:121-128. doi:10.1016/j. msea.2012.09.045
- [108] Edalati K, Yokoyama Y, Horita Z. High-pressure torsion of machining chips and bulk discs of amorphous $Zr_{50}Cu_{30}Al_{10}Ni_{10}$. Mater Trans. 2010;51:23–26. doi:10.2320/matertrans.MB200914
- [109] Edalati K, Horita Z. Universal plot for hardness variation in pure metals processed by high-pressure torsion. Mater Trans. 2010;51:1051-1054. doi:10.2320/ matertrans.M2009431
- [110] Rigney DA, Karthikeyan S. The evolution of tribomaterial during sliding: a brief introduction Tribol Lett. 2010;39:3-7. doi:10.1007/s11249-009-9498-3
- [111] Thomson W. XLVI. Hydrokinetic solutions and observations. London Edinburgh Dublin Philos 1871;42:362-377. Mag J Sci. doi:10.1080/ 14786447108640585
- [112] Helmholtz XLIII. XLIII. On discontinuous movements of fluids. London Edinburgh Dublin Philos 1868;36:337-346. Ţ Sci. 14786446808640073
- [113] Vo NQ, Zhou J, Ashkenazy Y, et al. Atomic mixing in metals under shear deformation. JOM. 2013;65:382-389. doi:10.1007/s11837-012-0542-7
- [114] Ashkenazy Y, Vo NQ, Schwen D, et al. Shear induced chemical mixing in heterogeneous systems. Acta Mater. 2012;60:984-993. doi:10.1016/j.actamat.2011. 11.014
- [115] Gente C, Oehring M, Bormann R. Formation of thermodynamically unstable solid solutions in the Cu-Co system by mechanical alloying. Phys Rev B. doi:10.1103/PhysRevB.48. 1993;48:13244-13252. 13244
- [116] Arshad SN, Lach TG, Pouryazdan M, et al. Dependence of shear-induced mixing on length scale. Scr Mater. 2013;68:215-218. doi:10.1016/j. scriptamat.2012.10.027
- [117] Veltl G, Scholz B, Kunze HD. Amorphization of CuTa alloys by mechanical alloying. Mater Sci Eng 1991;134:1410–1413. doi:10.1016/0921-5093 (91)91002-A
- [118] Bellon P, Averback RS. Nonequilibrium roughening of interfaces in crystals under shear: application to ball milling. Phys Rev Lett. 1995;74:1819-1822. doi:10.1103/PhysRevLett.74.1819



- [119] Straumal BB, Mazilkin AA, Baretzky B, et al. Accelerated diffusion and phase transformations in Co-Cu alloys driven by the severe plastic deformation. Mater Trans. 2012;53:63-71. doi:10.2320/ matertrans.MD201111
- [120] Divinski SV, Ribbe J, Baither D, et al. Nano- and micro-scale free volume in ultrafine grained Cu-1wt.%Pb alloy deformed by equal channel angular pressing. Acta Mater. 2009;57:5706-5717. doi:10. 1016/j.actamat.2009.07.066
- [121] Valiev RZ, Sergueeva AV, Mukherjee AK. The effect of annealing on tensile deformation behavior of nanostructured SPD titanium. Scr Mater. 2003;49:669-674. doi:10.1016/S1359-6462 (03)00395-6
- [122] Kumar P, Kawasaki M, Langdon TG. Review: overcoming the paradox of strength and ductility in ultrafine-grained materials at low temperatures. J Mater Sci. 2016;51:7-18. doi:10.1007/s10853-015-
- [123] Gubicza J, El-Tahawy M, Lábár JL, et al. Evolution of microstructure and hardness during artificial aging of an ultrafine-grained Al-Zn-Mg-Zr alloy processed by high pressure torsion. J Mater Sci. 2020;55:16791-16805. doi:10.1007/s10853-020-05264-4
- [124] Kormout KS, Ghosh P, Bachmaier A, et al. Effect of processing temperature on the microstructural characteristics of Cu-Ag nanocomposites: from supersaturation to complete phase decomposition. Acta Mater. 2018;154:33-44. doi:10.1016/j.actamat. 2018.05.010
- [125] Bachmaier A, Keckes J, Kormout KS, et al. Supersaturation in Ag-Ni alloy by two-step highpressure torsion processing. Philos Mag Lett. 2014;94:9-17. doi:10.1080/09500839.2013.852284
- [126] Edwards D, Sabirov I, Sigle W, et al. Microstructure and thermostability of a W-Cu nanocomposite produced via high-pressure torsion. Philos Mag. 2012;92:4151-4166. doi:10.1080/14786435.2012.
- [127] Sauvage X, Jessner P, Vurpillot F, et al. Nanostructure and properties of a Cu-Cr composite processed by severe plastic deformation. Scr Mater. 2008;58:1125–1128. doi:10.1016/j.scriptamat.2008. 02.010
- [128] Bachmaier A, Rathmayr GB, Bartosik M, et al. New insights on the formation of supersaturated solid solutions in the Cu-Cr system deformed by highpressure torsion. Acta Mater. 2014;69:301-313. doi:10.1016/j.actamat.2014.02.003
- [129] Bachmaier A, Kerber M, Setman D, et al. The formation of supersaturated solid solutions in Fe-Cu alloys deformed by high-pressure torsion. Acta Mater. 2012;60:860-871. doi:10.1016/j.actamat.2011.
- [130] Sauvage X, Pippan R. Nanoscaled structure of a Cu-Fe composite processed by high-pressure torsion. Mater Sci Eng A. 2005;410-411:345-347. doi:10. 1016/j.msea.2005.08.122
- [131] Bachmaier A, Pfaff M, Stolpe M, et al. Phase separation of a supersaturated nanocrystalline Cu-Co alloy and its influence on thermal stability. Acta Mater. 2015;96:269-283. doi:10.1016/j.actamat.2015.05.053
- [132] Han J-K, Liss K-D, Langdon TG, et al. Synthesis of a bulk nanostructured metastable Al alloy with extreme supersaturation of Mg. Sci Rep. 2019;9:17186. doi:10.1038/s41598-019-53614-3

- [133] Bachmaier A, Aboulfadl H, Pfaff M, et al. Structural evolution and strain induced mixing in Cu-Co composites studied by transmission electron microscopy and atom probe tomography. Mater Charact. 2015;100:178–191. doi:10.1016/j.matchar.2014.12.022
- Edalati K, Toh S, Arita M, et al. High-pressure torsion of pure cobalt: Hcp-fcc phase transformations and twinning during severe plastic deformation. Appl Phys Lett. 2013;102:181902. doi:10.1063/1.4804273
- [135] Li P, Gao G, Wang Y, et al. Crystal structures and exotic behavior of magnesium under pressure. J Phys Chem C. 2010;114:21745-21749. doi:10.1021/ jp108136r
- [136] Chen P, Wang F, Li B. Misfit strain induced phase transformation at a basal/prismatic twin boundary in deformation of magnesium. Comput Mater Sci. 2019;164:186-194. doi:10.1016/j.commatsci.2019.04.
- [137] López Gómez EI, Edalati K, Coimbrão DD, et al. FCC phase formation in immiscible Mg-Hf (magnesiumhafnium) system by high-pressure torsion. AIP Adv. 2020;10:055222. doi:10.1063/5.0009456
- [138] Zhang J, Guyot F. Experimental study of the bcc-fcc phase transformations in the Fe-rich system Fe-Si at high pressures. Phys Chem Miner. 1999;26:419-424. doi:10.1007/s002690050203
- [139] Janish MT, Kotula PG, Boyce BL, et al. Observations of fcc and hcp tantalum. J Mater Sci. 2015;50:3706-3715. doi:10.1007/s10853-015-8931-2
- [140] Einarsdotter K, Sadigh B, Grimvall G, et al. Phonon instabilities in fcc and bcc tungsten. Phys Rev Lett. 1997;79:2073-2076. doi:10.1103/PhysRevLett.79. 2073
- [141] Hoch M. The phase stability of body-centered cubic nickel, and face-centered cubic chromium. Calphad. 1993;17:157-160. doi:10.1016/0364-5916 (93)90016-5
- [142] Kormout KS, Pippan R, Bachmaier A. Deformationinduced supersaturation in immiscible material systems during high-pressure torsion. Adv Eng Mater. 2017;19:1600675. doi:10.1002/adem.201600675
- [143] Wilde G, Rösner H. Stability aspects of bulk nanostructured metals and composites. J Mater Sci. 2007;42:1772–1781. doi:10.1007/s10853-006-0986-7
- [144] Huang JY, Zhu YT, Liao XZ, et al. Amorphization of TiNi induced by high-pressure torsion. Philos Mag Lett. 2004;84:183-190. doi:10.1080/ 09500830310001657353
- [145] Sundeev RV, Glezer AM, Shalimova AV. Crystalline to amorphous transition in solids upon highpressure torsion. J Alloys Compd. 2014;611:292-296. doi:10.1016/j.jallcom.2014.05.109
- [146] Straumal BB, Mazilkin AA, Protasova SG, et al. Amorphization of crystalline phases in the Nd-Fe-B alloy driven by the high-pressure torsion. Mater Lett. 2015;161:735-739. doi:10.1016/j.matlet.2015. 09.076
- [147] Rogachev SO, Sundeev RV, Tabachkova NY. High pressure torsion-induced amorphous phase in a multilayer V-10Ti-5Cr/Zr-2.5Nb/V-10Ti-5Cr hybrid material. Mater Lett. 2019;234:220-223. doi:10. 1016/j.matlet.2018.09.112
- [148] Korznikov AV, Tram G, Dimitrov O, et al. The mechanism of nanocrystalline structure formation in Ni3Al during severe plastic deformation. Acta Mater. 2001;49:663-671. doi:10.1016/S1359-6454 (00)00345-1



- [149] Straumal B, Valiev R, Kogtenkova O, et al. Thermal evolution and grain boundary phase transformations in severely deformed nanograined Al-Zn alloys. Acta Mater. 2008;56:6123-6131. doi:10.1016/j.actamat. 2008.08.021
- Straumal BB, Protasova SG, Mazilkin AA, et al. Deformation-driven formation of equilibrium phases in the Cu-Ni alloys. J Mater Sci. 2012;47:360-367. doi:10.1007/s10853-011-5805-0
- [151] Bachmaier A, Motz C. On the remarkable thermal stability of nanocrystalline cobalt via alloying. Mater Sci Eng A. 2015;624:41-51. doi:10.1016/j. msea.2014.11.062
- [152] Sun YF, Nakamura T, Todaka Y, et al. Fabrication of CuZr(Al) bulk metallic glasses by high pressure torsion. Intermetallics. 2009;17:256-261. doi:10.1016/j. intermet.2008.07.023
- [153] Straumal BB, Kilmametov AR, Mazilkin AA, et al. Transformations of Cu(in) supersaturated solid solutions under high-pressure torsion. Mater Lett. 2015;138:255-258. doi:10.1016/j.matlet.2014.10.009
- [154] Brandes EA, Brook GB. Smithells metals reference book. 7th ed. Oxford: Butterworth-Heinemann; 2004; doi:10.1016/B978-075067509-3/50014-2
- [155] Eizadjou M, Kazemi Talachi A, Danesh Manesh H, et al. Investigation of structure and mechanical properties of multi-layered Al/Cu composite produced by accumulative roll bonding (ARB) process. Compos Sci Technol. 2008;68:2003-2009. doi:10.1016/j. compscitech.2008.02.029
- [156] Yousefi Mehr V, Toroghinejad MR, Rezaeian A. Mechanical properties and microstructure evolutions of multilayered Al-Cu composites produced by accumulative roll bonding process and subsequent annealing. Mater Sci Eng A. 2014;601:40-47. doi:10. 1016/j.msea.2014.02.023
- [157] Abd El Aal MI, El Mahallawy N, Shehata FA, et al. Wear properties of ECAP-processed ultrafine grained Al-Cu alloys. Mater Sci Eng A. 2010;527:3726-3732. doi:10.1016/j.msea.2010.03.057
- [158] Murayama M, Horita Z, Hono K. Microstructure of two-phase Al-1.7 at% Cu alloy deformed by equalchannel angular pressing. Acta Mater. 2001;49:21-29. doi:10.1016/S1359-6454(00)00308-6
- [159] Kawasaki M, Alhajeri SN, Xu C, et al. The development of hardness homogeneity in pure aluminum and aluminum alloy disks processed by highpressure torsion. Mater Sci Eng A. 2011;529:345-351. doi:10.1016/j.msea.2011.09.039
- [160] Lee H-J, Ahn B, Kawasaki M, et al. Evolution in hardness and microstructure of ZK60A magnesium alloy processed by high-pressure torsion. J Mater Res Technol. 2015;4:18-25. doi:10.1016/J.JMRT.2014.10.
- [161] Huang Y, Kawasaki M, Langdon TG. An investigation of flow patterns and hardness distributions using different anvil alignments in high-pressure torsion. J Mater Sci. 2013;48;4533-4542. doi:10.1007/ s10853-012-7015-9
- [162] Wu K, Chang H, Maawad E, et al. Microstructure and mechanical properties of the Mg/Al laminated composite fabricated by accumulative roll bonding (ARB). Mater Sci Eng A. 2010;527:3073-3078. doi:10.1016/j.msea.2010.02.001
- [163] Liu HS, Zhang B, Zhang GP. Microstructures and mechanical properties of Al/Mg alloy multilayered composites produced by accumulative roll bonding.

- J Mater Sci Technol. 2011;27:15-21. doi:10.1016/ S1005-0302(11)60019-4
- [164] Chang H, Zheng MY, Xu C, et al. Microstructure and mechanical properties of the Mg/Al multilayer fabricated by accumulative roll bonding (ARB) at ambient temperature. Mater Sci Eng A. 2012;543:249-256. doi:10.1016/j.msea.2012.02.083
- [165] Fang DR, Duan QQ, Zhao NQ, et al. Tensile properties and fracture mechanism of Al-Mg alloy subjected to equal channel angular pressing. Mater Sci Eng A. 2007;459:137–144. doi:10.1016/j.msea.2007. 01.062
- [166] Xu J, Shirooyeh M, Wongsa-Ngam J, et al. Hardness homogeneity and micro-tensile behavior in a magnesium AZ31 alloy processed by equal-channel angular pressing. Mater Sci Eng A. 2013;586:108-114. doi:10.1016/j.msea.2013.07.096
- [167] Chang S-Y, Lee S-W, Kang KM, et al. Improvement of mechanical characteristics in severely plasticdeformed Mg alloys. Mater Trans. 2004;45:488-492. doi:10.2320/matertrans.45.488
- [168] Pospíšilová I, Vojtěch D. Mechanical properties of Zn-Mg alloys. Metal. 2013;15:15-17.
- [169] Dambatta MS, Izman S, Kurniawan D, et al. Processing of Zn-3Mg alloy by equal channel angular pressing for biodegradable metal implants. J King Saud Univ - Sci. 2017;29:455-461. doi:10.1016/j. iksus.2017.07.008
- [170] Sanaty-Zadeh A. Comparison between current models for the strength of particulate-reinforced metal matrix nanocomposites with emphasis on consideration of Hall-Petch effect. Mater Sci Eng A. 2012;531:112-118. doi:10.1016/j.msea.2011.10.043
- [171] Arsenault RJ, Shi N. Dislocation generation due to differences between the coefficients of thermal expansion. Mater Sci Eng. 1986;81:175-187. doi:10. 1016/0025-5416(86)90261-2
- [172] Casati R, Vedani M. Metal matrix composites reinforced by nano-particles-A review. Metals (Basel). 2014;4:65-83. doi:10.3390/met4010065
- [173] Miller WS, Humphreys FJ. Strengthening mechanisms in particulate metal matrix composites. Scr Metall Mater. 1991;25:33-38. doi:10.1016/0956-716X(91)90349-6
- [174] Joo SH, Yoon SC, Lee CS, et al. Microstructure and tensile behavior of Al and Al-matrix carbon nanotube composites processed by high pressure torsion of the powders. J Mater Sci. 2010;45:4652-4658. doi:10.1007/s10853-010-4382-y
- Sathiyamoorthi P, Bae J, Asghari-Rad P, et al. Effect of annealing on microstructure and tensile behavior of CoCrNi medium entropy alloy processed by high-pressure torsion. Entropy. 2018;20:849. doi:10. 3390/e20110849
- [176] Praveen S, Bae JW, Asghari-Rad P, et al. Ultra-high tensile strength nanocrystalline CoCrNi equi-atomic medium entropy alloy processed by high-pressure torsion. Mater Sci Eng A. 2018;735:394-397. doi:10. 1016/j.msea.2018.08.079
- Xu J, Wang X, Shirooyeh M, et al. Microhardness, microstructure and tensile behavior of an AZ31 magnesium alloy processed by high-pressure torsion. J Mater Sci. 2015;50:7424-7436. doi:10.1007/s10853-015-9300-x
- [178] Yilmazer H, Niinomi M, Nakai M, et al. Mechanical properties of a medical β-type titanium alloy with specific microstructural evolution through high-



- pressure torsion. Mater Sci Eng C. 2013;33:2499-2507. doi:10.1016/j.msec.2013.01.056
- [179] Müller T, Kapp MW, Bachmaier A, et al. Ultrahighstrength low carbon steel obtained from the martensitic state via high pressure torsion. Acta Mater. 2019;166:168–177. doi:10.1016/j.actamat.2018.12.028
- [180] Edalati K, Horita Z, Yagi S, et al. Allotropic phase transformation of pure zirconium by high-pressure torsion. Mater Sci Eng A. 2009;523:277-281. doi:10. 1016/J.MSEA.2009.07.029
- [181] Khatibi G, Horky J, Weiss B, et al. High cycle fatigue behaviour of copper deformed by high pressure torsion. Int J Fatigue. 2010;32:269–278. doi:10.1016/j. ijfatigue.2009.06.017
- [182] Murashkin M, Sabirov I, Prosvirnin D, et al. Fatigue behavior of an ultrafine-grained Al-Mg-Si alloy processed by high-pressure torsion. Metals (Basel). 2015;5:578-590. doi:10.3390/met5020578
- [183] Choi IC, Yoo BG, Kraft O, et al. High-cycle fatigue behavior of Zn-22% Al alloy processed by highpressure torsion. Mater Sci Eng A. 2014;618:37-40. doi:10.1016/j.msea.2014.08.084
- [184] Zhang W, Simpson CA, Leitner T, et al. The effect of anisotropic microstructure on the crack growth and fatigue overload behaviour of ultrafine-grained nickel. Acta Mater. 2020;184:225-240. doi:10.1016/j. actamat.2019.11.024
- [185] Leitner T, Hohenwarter A, Pippan R. Fatigue crack growth behavior of ultrafine-grained nickel produced by high pressure torsion. Procedia Mater Sci. 2014;3:1044-1049. doi:10.1016/j.mspro.2014.06.170
- [186] Horky J, Khatibi G, Setman D, et al. Effect of microstructural stability on fatigue crack growth behaviour of nanostructured Cu. Mech Mater. 2013;67:38-45. doi:10.1016/j.mechmat.2013.07.008
- [187] Long BD, Umemoto M, Todaka Y, et al. Fabrication of high strength Cu-NbC composite conductor by high pressure torsion. Mater Sci Eng A. 2011;528:1750-1756. doi:10.1016/J.MSEA.2010.11.
- [188] Bazarnik P, Bartkowska A, Romelczyk-Baishya B, et al. Superior strength of tri-layered Al-Cu-Al nano-composites processed by high-pressure torsion. J Alloys Compd. 2020;846:156380. doi:10.1016/j. jallcom.2020.156380
- [189] Tabor D. The hardness of solids. Rev Phys Technol. 1970;1:145–179. doi:10.1088/0034-6683/1/3/I01
- [190] Picu RC. A mechanism for the negative strain-rate sensitivity of dilute solid solutions. Acta Mater. 2004;52:3447–3458. doi:10.1016/j.actamat.2004.03.
- [191] Valiev RZ, Alexandrov IV, Zhu YT, et al. Paradox of strength and ductility in metals processed bysevere plastic deformation. J Mater Res. 2002;17:5-8. doi:10.1557/JMR.2002.0002
- [192] Valiev R. Materials science: nanomaterial advantage. Nature. 2002;419:887-889. doi:10.1038/419887a
- [193] Hart EW. Theory of the tensile test. Acta Metall. 1967;15:351–355. doi:10.1016/0001-6160(67)90211-8
- [194] Wang YM, Ma E. Strain hardening, strain rate sensitivity, and ductility of nanostructured metals. Mater Sci Eng A. 2004;375-377:46-52. doi:10.1016/j.msea. 2003.10.214
- [195] Han JK, Herndon T, il Jang J, et al. Synthesis of hybrid nanocrystalline alloys by mechanical bonding through high-pressure torsion. Adv Eng Mater. 2020;22:1901289. doi:10.1002/adem.201901289

- [196] Wang YC, Langdon TG. Effect of heat treatment on microstructure and microhardness evolution in a Ti-6Al-4V alloy processed by high-pressure torsion. J Mater Sci. 2013;48:4646-4652. doi:10.1007/s10853-012-7071-1
- [197] Torbati-Sarraf SA, Sabbaghianrad S, Figueiredo RB, et al. Orientation imaging microscopy and microhardness in a ZK60 magnesium alloy processed by highpressure torsion. J Alloys Compd. 2017;712:185–193. doi:10.1016/J.JALLCOM.2017.04.054
- [198] Kawasaki M, Figueiredo RB, Huang Y, et al. Interpretation of hardness evolution in metals processed by high-pressure torsion. J Mater Sci. 2014;49:6586–6596. doi:10.1007/s10853-014-8262-8
- [199] Chinh NQ, Csanádi T, Gubicza J, et al. The effect of grain boundary sliding and strain rate sensitivity on the ductility of ultrafine-grained materials. Mater Sci Forum. 2010;667-669:677-682. doi:10.4028/ www.scientific.net/MSF.667-669.677
- [200] Wu X, Zhu Y. Heterogeneous materials: a new class of materials with unprecedented mechanical properties. Mater Res Lett. 2017;5:527-532. doi:10.1080/ 21663831.2017.1343208.
- [201] Asghari-Rad P, Sathiyamoorthi P, Thi-Cam Nguyen N, et al. Fine-tuning of mechanical properties in V10Cr15Mn5Fe35Co10Ni25 high-entropy alloy through high-pressure torsion and annealing. Mater Sci Eng A. 2020;771:138604. doi:10.1016/j.msea. 2019.138604
- [202] Asghari-Rad P, Sathiyamoorthi P, Nguyen NTC, et al. A powder-metallurgy-based fabrication route towards achieving high tensile strength with ultrahigh ductility in high-entropy alloy. Scr Mater. 2021;190:69-74. doi:10.1016/j.scriptamat.2020.08. 038
- [203] Akbarpour MR, Mousa Mirabad H, Alipour S, et al. Enhanced tensile properties and electrical conductivity of Cu-CNT nanocomposites processed via the combination of flake powder metallurgy and high pressure torsion methods. Mater Sci Eng A. 2020;773:138888. doi:10.1016/j.msea.2019.138888
- [204] Ren ZQ, Churakova AA, Wang X, et al. Enhanced tensile strength and ductility of bulk metallic glasses Zr52.5Cu17.9Al10Ni14.6Ti5 via high-pressure torsion. Mater Sci Eng A. 2021;803:140485. doi:10. 1016/j.msea.2020.140485
- [205] Watroba M, Bednarczyk W, Kawałko J, et al. A novel high-strength Zn-3Ag-0.5Mg alloy processed by hot extrusion, cold rolling, or high-pressure torsion. Metall Mater Trans A Phys Metall Mater Sci. 2020;51:3335-3348. doi:10.1007/s11661-020-05797-y
- Kawabata H, Aoi I, Oh-Ishi K, et al. Improved combination of strength and ductility in zirconiumadded Al-Zn-Mg-Cu alloy processed with highpressure torsion. Mater Trans. 2016;57:1735-1740. doi:10.2320/matertrans.M2016215
- [207] Liu M, Zheng R, Li J, et al. Achieving ultrahigh tensile strength of 1 GPa in a hierarchical nanostructured 2024 Al alloy. Mater Sci Eng A. 2020;788:139576. doi:10.1016/j.msea.2020.139576
- [208] Liu Y, He Y, Cai S. Effect of gradient microstructure on the strength and ductility of medium-entropy alloy processed by severe torsion deformation. Mater Sci Eng A. 2021;801:140429. doi:10.1016/j. msea.2020.140429
- [209] Zhang X, Huang LK, Zhang B, et al. Microstructural evolution and strengthening mechanism of an Al-Si-

- - Mg alloy processed by high-pressure torsion with different heat treatments. Mater Sci Eng A. 2020;794:139932. doi:10.1016/j.msea.2020.139932
- [210] An XH, Wu SD, Zhang ZF, et al. Enhanced strengthductility synergy in nanostructured Cu and Cu-Al alloys processed by high-pressure torsion and subsequent annealing. Scr Mater. 2012;66:227–230. doi:10.1016/J.SCRIPTAMAT.2011.10.043
- [211] Liu M, Zheng R, Ma C, et al. Ultra-strong, ductile and thermally stable ultrafine grained 5083 Al alloy fabricated by high pressure torsion using pre-sintered powders. Materialia. 2019;8:100448. doi:10.1016/j. mtla.2019.100448
- [212] Shi S, Zhang Z, Wang X, et al. Microstructure evolution and enhanced mechanical properties in SUS316LN steel processed by high pressure torsion at room temperature. Mater Sci Eng A. 2018;711:476–483. doi:10.1016/j.msea.2017.11.064
- [213] Kang JY, Kim JG, Park HW, et al. Multiscale architectured materials with composition and grain size gradients manufactured using high-pressure torsion. Sci Rep. 2016;6:26590. doi:10.1038/srep26590
- [214] Estrin Y, Beygelzimer Y, Kulagin R. Design of architectured materials based on mechanically driven structural and compositional patterning. Adv Eng Mater. 2019;21:1900487. doi:10.1002/adem.201900487
- [215] Beygelzimer Y, Kulagin R, Estrin Y. Severe plastic deformation as a way to produce architectured materials. Springer Ser Mater Sci Springer Verlag. 2019;282:231-255. doi:10.1007/978-3-030-11942-3_8
- [216] Hernández-Escobar D, Champagne S, Yilmazer H, et al. Current status and perspectives of zinc-based absorbable alloys for biomedical applications. Acta Biomater. 2019;97:1-22. doi:https://doi.org/10.1016/ j.actbio.2019.07.034
- [217] Vojtěch D, Kubásek J, Šerák J, et al. Mechanical and corrosion properties of newly developed biodegradable Zn-based alloys for bone fixation. Acta 2011;7:3515-3522. Biomater. doi:10.1016/J. ACTBIO.2011.05.008
- [218] Zheng YF, Gu XN, Witte F. Biodegradable metals. Mater Sci Eng R Reports. 2014;77:1-34. doi:10. 1016/J.MSER.2014.01.001
- [219] Bowen PK, Guillory RJ, Shearier ER, et al. Metallic zinc exhibits optimal biocompatibility for bioabsorbable endovascular stents. Mater Sci Eng C. 2015;56:467-472. doi:10.1016/j.msec.2015.07.022
- [220] Yang H, Wang C, Liu C, et al. Evolution of the degradation mechanism of pure zinc stent in the one-year study of rabbit abdominal aorta model. Biomaterials. 2017;145:92-105. doi:10.1016/J.BIOMATERIALS. 2017.08.022
- [221] Dambatta MS, Kurniawan D, Izman S, et al. Review on Zn-based alloys as potential biodegradable medical devices materials. Appl Mech Mater. 2015;776:277-281. doi:10.4028/www.scientific.net/ AMM.776.277
- [222] Katarivas Levy G, Goldman J, Aghion E. The prospects of zinc as a structural material for biodegradable implants—a review paper. Metals (Basel). 2017;7:402. doi:10.3390/met7100402
- [223] Mostaed E, Sikora-Jasinska M, Drelich JW, et al. Zinc-based alloys for degradable vascular stent applications. Acta Biomater. 2018;71:1-23. doi:10.1016/J. ACTBIO.2018.03.005
- [224] Venezuela J, Dargusch MS. The influence of alloying and fabrication techniques on the mechanical

- properties, biodegradability and biocompatibility of zinc: a comprehensive review. Acta Biomater. 2019;87:1–40. doi:10.1016/J.ACTBIO.2019.01.035
- [225] Čapek J, Jablonská E, Lipov J, et al. Preparation and characterization of porous zinc prepared by spark plasma sintering as a material for biodegradable scaffolds. Mater Chem Phys. 2018;203:249-258. doi:10.1016/J.MATCHEMPHYS.2017.10.008
- [226] Bowen PK, Drelich J, Goldman J. Zinc exhibits ideal physiological corrosion behavior for bioabsorbable stents. Adv Mater. 2013;25:2577-2582. doi:10.1002/ adma.201300226
- [227] Zhao L, Wang X, Wang T, et al. Mechanical properties and biodegradation of porous Zn-1Al alloy scaffolds. Mater Lett. 2019;247:75-78. doi:10.1016/J. MATLET.2019.03.097
- [228] Zhang C, Guan S, Wang L, et al. Effect of solution pretreatment on homogeneity and corrosion resistance of biomedical Mg-Zn-Ca alloy processed by pressure torsion. Adv Eng 2017;19:1600326. doi:10.1002/adem.201600326
- [229] Zhang CZ, Zhu SJ, Wang LG, et al. Microstructures and degradation mechanism in simulated body fluid of biomedical Mg-Zn-Ca alloy processed by high pressure torsion. Mater Des. 2016;96:54-62. doi:10.1016/j.matdes.2016.01.072
- [230] Isik M, Niinomi M, Cho K, et al. Microstructural evolution and mechanical properties of biomedical Co-Cr-Mo alloy subjected to high-pressure torsion. J Mech Behav Biomed Mater. 2016;59:226-235. doi:10.1016/j.jmbbm.2015.11.015
- [231] Yilmazer H, Niinomi M, Nakai M, et al. Heterogeneous structure and mechanical hardness of biomedical -type Ti-29Nb-13Ta-4.6Zr subjected to high-pressure torsion. J Mech Behav Biomed Mater. 2012;10:235-245. doi:10.1016/j.jmbbm.2012. 02.022
- [232] Yilmazer H, Şen M, Niinomi M, et al. Developing biomedical nano-grained β-type titanium alloys using high pressure torsion for improved cell adherence. RSC Adv. 2016;6:7426-7430. doi:10.1039/
- [233] Faghihi S, Zhilyaev AP, Szpunar JA, et al. Nanostructuring of a titanium material by highpressure torsion improves pre-osteoblast attachment. Adv Mater. 2007;19:1069-1073. doi:10.1002/adma. 200602276
- [234] Faghihi S, Azari F, Zhilyaev AP, et al. Cellular and molecular interactions between MC3T3-E1 pre-osteoblasts and nanostructured titanium produced by highpressure torsion. Biomaterials. 2007;28:3887-3895. doi:10.1016/j.biomaterials.2007.05.010
- [235] Campos-Quirós A, Cubero-Sesín JM, Edalati K. Synthesis of nanostructured biomaterials by highpressure torsion: Effect of niobium content on microstructure and mechanical properties of Ti-Nb alloys. Mater Sci Eng A. 2020;795:139972. doi:10.1016/j. msea.2020.139972
- [236] Panigrahi A, Sulkowski B, Waitz T, et al. Mechanical properties, structural and texture evolution of biocompatible Ti-45Nb alloy processed by severe plastic deformation. J Mech Behav Biomed Mater. 2016;62:93-105. doi:10.1016/j.jmbbm.2016.04.042
- [237] Nieto A, Bisht A, Lahiri D, et al. Graphene reinforced metal and ceramic matrix composites: a review. Int Mater Rev. 2017;62:241-302. doi:10.1080/09506608. 2016.1219481



- [238] Bachmaier A, Pippan R. High-pressure torsion deformation induced phase transformations and formations: New material combinations and advanced properties. Mater Trans. 2019;60:1256-1269. doi:10. 2320/matertrans.MF201930
- [239] Cubero-Sesin JM, Arita M, Horita Z. High strength and electrical conductivity of Al-Fe alloys produced by synergistic combination of high-pressure torsion and aging. Adv Eng Mater. 2015;17:1792-1803. doi:10.1002/adem.201500103
- [240] Berkowitz AE, Mitchell JR, Carey MJ, et al. Giant magnetoresistance in heterogeneous Cu-Co alloys. Phys Rev Lett. 1992;68:3745-3748. doi:10.1103/ PhysRevLett.68.3745
- [241] Straumal BB, Protasova SG, Mazilkin AA, et al. SPDinduced changes of structure and magnetic properties in the Cu-Co alloys. Mater Lett. 2013;98:217-221. doi:10.1016/j.matlet.2013.02.058
- [242] Popov AG, Gaviko VS, Shchegoleva NN, et al. Highpressure-torsion deformation of Nd9Fe85B6 alloy. Phys Met Metallogr. 2007;104:238–247. doi:10.1134/S0031918X07090050
- [243] Straumal BB, Kilmametov AR, Mazilkin AA, et al. Amorphization of Nd-Fe-B alloy under the action of high-pressure torsion. Mater Lett. 2015;145:63-66. doi:10.1016/j.matlet.2015.01.041
- [244] Popov AG, Gaviko VS, Shchegoleva NN, et al. Effect of high-pressure torsion deformation and subsequent annealing on structure and magnetic properties of overquenched melt-spun Nd9Fe85B6 alloy. J Iron Steel Res Int. 2006;13:160-165. doi:10.1016/S1006-706X(08)60175-2
- [245] Stolyarov VV, Gunderov DV, Popov AG, et al. Structure evolution and changes in magnetic

- properties of severe plastic deformed Nd(Pr)-Fe-B alloys during annealing. J Alloys Compd. 1998;281:69-71. doi:10.1016/S0925-8388(98)00774-9
- Li H, Lou L, Hou F, et al. Simultaneously increasing the magnetization and coercivity of bulk nanocomposite magnets via severe plastic deformation. Appl Phys Lett. 2013;103:142406. doi:10.1063/1.4824032
- Cepeda-Jiménez CM, Beltrán JI, Hernando A, et al. Tuning the magnetic properties of pure hafnium by high pressure torsion. Acta Mater. 2017;123:206-213. doi:10.1016/j.actamat.2016.10.052
- [248] Edalati K, Akiba E, Horita Z. High-pressure torsion for new hydrogen storage materials. Sci Technol Adv Mater. 2018;19:185-193. doi:10.1080/14686996. 2018.1435131
- [249] Edalati K, Emami H, Staykov A, et al. Formation of metastable phases in magnesium-titanium system by high-pressure torsion and their hydrogen storage performance. Acta Mater. 2015;99:150-156. doi:10. 1016/j.actamat.2015.07.060
- [250] Emami H, Edalati K, Staykov A, et al. Solid-state reactions and hydrogen storage in magnesium mixed with various elements by high-pressure torsion: experiments and first-principles calculations. RSC Adv. 2016;6:11665-11674. doi:10.1039/c5ra23728a
- [251] Edalati K, Emami H, Ikeda Y, et al. New nanostructured phases with reversible hydrogen storage capability in immiscible magnesium-zirconium system produced by high-pressure torsion. Acta Mater. 2016;108:293-303. doi:10.1016/j.actamat.2016.02.026
- [252] Edalati K, Uehiro R, Ikeda Y, et al. Design and synthesis of a magnesium alloy for room temperature hydrogen storage. Acta Mater. 2018;149:88-96. doi:10.1016/j.actamat.2018.02.033